The Global Forest Fire Emissions Prediction System version 1.0

Kerry Anderson[1,2], Jack Chen[1], Peter Englefield[3], Debora Griffin[1], Paul A. Makar[1], Dan Thompson[4]

[1] Air Quality Research Division, Environment and Climate Change Canada, Toronto, Ontario, Canada
[2] Natural Resources Canada (emeritus)
5   [3] Natural Resources Canada, Edmonton, Alberta, Canada
[4] Natural Resources Canada, Sault St. Marie, Ontario, Canada

Correspondence to: Kerry Anderson (kerryanderson@shaw.ca)

Abstract. The Global Forest Fire Emissions Prediction System (GFFEPS) is a model that estimates biomass burning in real time for global air-quality forecasting. The model uses a bottom-up approach, based on remotely-sensed hotspot locations,
10   and global databases linking burned area per hotspot to ecosystem-type classification at a 1-km resolution. Unlike other global forest fire emissions models, GFFEPS provides dynamic estimates of fuel consumption and fire behaviour based on the Canadian Forest Fire Danger Rating System. Combining forecasts of daily fire weather and hourly meteorological conditions with a global land classification, GFFEPS produces fuel consumption and emission predictions in 3-hour time steps (in contrast to non-dynamic models that use fixed consumption rates and require collection of burned area to make post-burn estimates of
15   emissions). GFFEPS has been designed for use in near-real-time forecasting applications as well as historical simulations for which data are available. A study was conducted running GFFEPS through a six-year period (2015-2020). Regional annual total smoke emissions, burned area and total fuel consumption per unit area as predicted by GFFEPS were generated to assess model performance over multiple years and regions. The model distinguished grass-dominated regions from forested, while also showed high variability in regions affected by El Niño and deforestation. GFFEPS carbon emissions and burned area
20   were then compared to other global wildfire emissions models, including GFAS, GFED4.1s and FINN1.5/2.5. GFFEPS estimated values lower than GFAS/GFED (80%/74%), and estimated values similar to FINN1.5 (97%). This was largely due to the impact of fuel moisture on consumption rates as captured by the dynamic weather modelling. An effort is underway to validate the model, with further developments and improvements expected.

1 Introduction

25   Biomass burning from wildland fires and agricultural burning is a major source of carbon emissions and greenhouse gases globally. In 2021, estimates of emissions from wildland fire, deforestation and agricultural burning accounted for 1.84 Pg C yr^{-1} (Kaiser and van der Werf, 2022). Compared to the total anthropogenic emissions of 11.0 Pg C yr^{-1} (40.2 Pg CO_2 yr^{-1}, Friedlingstein et al., 2022), biomass burning would amount to 16% of global emissions; yet much of these emissions (1.75 Pg C yr^{-1} averaged over 2012–2021; Friedlingstein et al., 2022) are recaptured by carbon uptake in the forests (afforestation,
30   reafforestation and forestry) reducing their impact on global concentrations.

Unlike anthropogenic sources, emissions vary greatly from year to year as wildland fire is a dynamic and highly variable event. Estimates show that between 2003 to 2017, biomass burning accounted for 1.68 to 2.27 Pg C yr^{-1} (Kaiser and van der Werf, 2019). Recent events include:

- El Niño events (1997, 2006, 2015, 2019) that triggered extreme emissions from peat fires in Indonesia and southeast Asia (Field et al., 2009; Huijnen et al., 2016; Page and Hooijer, 2016);
- Australia's unprecedented fire season in 2019/2020, following its hottest, driest year on record (Abrams et al., 2021);
- California's record-breaking number of large fires in 2020, exceeding the previous record in 2018 (Keeley and Syphard, 2021);
- Canada's burned area reaching 76,129 km^2 on June 26, 2023, exceeding the previous record of 75,596 km^2 set for the entire year in 1989 (Lowrie, 2023) and ultimately reaching 184,961 km² by the close of 2023 (https://ciffc.net/situation/, last accessed 2023-12-05).

Wildfires also emit significant quantities of shorter-lived atmospheric pollutants (e.g., nitrogen oxides, volatile organic gases, carbon monoxide, ammonia, particulate matter, heavy metals; cf. Akagi et al., 2011, Urbanski, 2014, Hatch et al., 2017, Wentworth et al., 2018, Hayden et al., 2022, Liu et al., 2023). Global forest fire emissions of particulate matter have been identified as one of the largest sources of atmospheric trace gases and aerosols (Knorr et al., 2012), and their global particulate matter emissions have been found to result in 65.6 million deaths annually (Chen et al., 2021). Respiratory and cardiovascular deaths have been found to be among the chief causes of global wildfire PM mortality (Chen et al., 2021; Barros et al., 2023; Matz et al., 2020) and the impacts on the heart have been found to extend over several days subsequent to wildfire emissions exposure (Barros et al., 2023). Accurate emission estimates of wildfires for smoke forecasting and inventory accounting are therefore of great importance from the standpoint of assessing their impacts on human health and the environment.

Efforts to model wildfire emissions globally have been on-going since the 1970s (Seiler and Crutzen, 1980). Currently, several global wildfire emissions models exist (Pan et al., 2020), such as the Global Fire Analysis System (GFAS, Kaiser et al., 2012), the Global Fire Emissions Database (GFED, Van der Werf et al., 2017), the Fire INventory from NCAR (FINN, Wiedinmyer et al., 2011, Wiedinmyer et al., 2023) and others. Carbon emissions from GFAS (calibrated to partly match GFED emissions) are routinely used to estimate annual carbon emissions from wildland fires for the American Meteorological Society's annual State of the Climate reports (Kaiser and van der Werf, 2022). Wildfire emissions models are also used in conjunction with global chemical transport models such as the Copernicus Atmospheric Monitoring System (CAMS), which uses GFAS emissions to provide concentration estimates that are linked to human health outcomes (Roberts and Wooster, 2021).

Emissions models follow one of two general methodologies: either a top-down or a bottom-up approach to modelling. The top-down approach used by GFAS is centered around the satellite-based MODIS active fire products (the MOD14/MYD14 Level-2) that provide instantaneous observations of actively burning fires and measurements of fire radiative energy (FRE;

Mota and Wooster, 2018). The time integral of FRE (as fire radiative power, FRP) and biome-specific conversion factors are
65 used to determine combustion rates, which in turn are combined with emission factors to estimate emission rates. The bottom-
up approach used by GFED and FINN is based on the product of observed burned area (based on MODIS MCD64A1 mapping
algorithm), fuel loads, combustions completeness and emission factors. Both top-down and bottom-up methodologies use
satellite sensors for fire detection (MODIS and/or VIIRS) to identify fire locations spatially and temporally (Giglio et al.,
2016).

70   Each approach has its limitations. The satellite-based fire detection used by both top-down and bottom-up methodologies
are restricted by satellite-overpass times, sensor resolution, observational swath width, heavy smoke and cloud cover. The
bottom-up approach is also limited by land-cover and burned-area mapping resolution as well as the accuracy of fuel load
mapping and fuel consumption modelling. A methodology to extrapolate the contribution of small, undetected fires –
especially important for capturing cropland burning – was presented by Randerson et al. (2012) and included in GFED4.1s.
75 The effectiveness of this small fire boost to emissions has been questioned (Zhang et al., 2018; Gaveau et al., 2021; Ramo et
al., 2021) and so GFED5 was developed with scalar corrections based on higher-resolution (non-global) datasets from Landsat
and Sentinel-2 (Chen et al., 2023). Also, Van Wees et al. (2022) incorporated monthly water and temperature stress scalars to
model the net primary production (NPP) of stem, leaf and root pools at a 500-m spatial resolution into a simplified version the
GFED model, giving fuel loads a temporal variability.

80   A second limitation of current models is the use of static values for combustion completeness. Fire behaviour is
recognized as being dependent on fuels, weather and topography, with weather in the form of temperature, wind, humidity,
precipitation, cloud cover and atmospheric stability, being the most variable (Countryman, 1972). The Canadian Forest Fire
Danger Rating System (CFFDRS, Stocks et al., 1989) addresses these factors daily in the Canadian Forest Fire Weather Index
(FWI) System (Van Wagner, 1987), a system that has seen uptake not only in North America but also New Zealand, Mexico,
85 parts of Europe and southeast Asia (Taylor and Alexander 2006).

      The Canadian Forest Fire Emissions Prediction System (CFFEPS) is a model that predicts smoke emissions for North
America based on the CFFDRS. Driven by forecasted hourly meteorology at hotspot locations, the model estimates the hourly
chemical components of fire emissions, the plume injection height and vertical distribution of emissions. Predicted smoke
emissions are incorporated into Environment and Climate Change Canada's numerical weather and chemical transport model
90 (the Global Environmental Multiscale – Modelling Air quality and Chemistry model; GEM-MACH). The combined system
of emissions and transport is referred to as FireWork. The plume rise component of CFFEPS, as derived from modelled fuel
consumption, has been extensively validated using satellite plume height observations (Griffin et al., 2019). As part of
FireWork, the CFFEPS model has been incorporated into ECCC's operational Air Quality Health Index (AQHI) forecasts for
North America since 2019 (Chen et al., 2019). More recent work with CFFEPS has allowed its incorporation on-line into a
95 research version of the GEM-MACH two-way coupled air-quality model, in turn accounting for aerosol feedbacks between
wildfire emissions and regional weather to be simulated (Makar et al., 2020).

This paper describes the adaptation and extension of the methodologies used in the CFFEPS model to a global domain, as the Global Forest Fire Emissions Prediction System (GFFEPS) – a system that provides spatiotemporal forest fire emissions estimates based on satellite hotspot retrievals, weather and fire behaviour modelling at the global scale. The motivation for
100   this work was the recognized need in extending FireWork's current North American air-quality forecasting to the global domain. With increasing fire frequency, size and intensity, smoke can be injected aloft and transported across oceans. For example, smoke from the 2016 Fort McMurray Fire (a.k.a. the Horse River Fire, 2016) affected New York (Wu et al., 2018) and reached as far as the United Kingdom (Vaughan et al., 2018); similarly, the 2023 wildfires in Quebec were observed to transport across the Atlantic impacting air quality of many European communities. A recent study (Makar et al., 2020) showed
105   the impact of forest fire smoke emissions from Eurasia on North American meteorology and air quality forecasting, highlighting that un-nested continental-only scale air quality models show reduced skill during transoceanic smoke transport events. The impacts of intercontinental pollutant transport have also been demonstrated elsewhere in the literature (e.g., Huang et al., 2017). This paper sets out to document the data, the methodology and resulting predictions of the GFFEPS model, comparing it to other published global fire emissions models as a first step towards larger validation efforts.

110   **2 Theory**

A central problem of predicting smoke emissions is the estimation of the amount of forest fuel consumed by fire, which in turn is injected into the atmosphere. For the bottom-up approach, estimating the amount of fuel consumed involves estimating the total mass of biomass combustion, which is the product of fuel consumed per unit area (kg m^{-2} or t ha^{-1}) and burned area (m^2, ha or km^2). The emissions of specific gas and particle species (collectively, "tracers") is estimated from final
115   effective mass of fuel consumed multiply by emission factors. Emissions factors are generally pre-determined values derived from measurements as mass of species emitted per unit mass of fuel consumed, typically grams of emitted species per kg of dry fuel consumed (Urbanski, 2014). Fuel consumed is used to calculate total heat flux from the combustion process and then used to calculate plume injection height, and parameterize the vertical distribution of the emitted tracers for distribution within a vertical atmospheric column. Species are distributed from the surface to the plume height based on maintaining a constant
120   mixing ratio of smoke to clean air. The process and unit convention used in the paper is illustrated in Fig. 1.
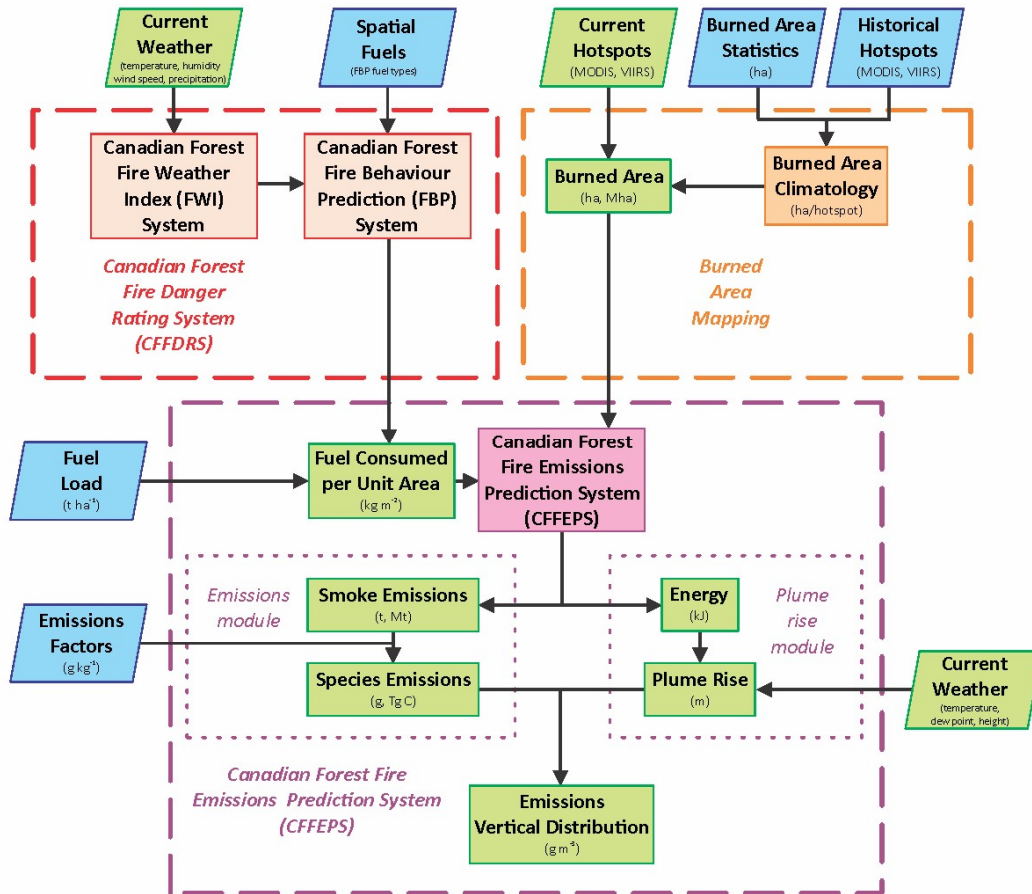
Figure 1. Structure of the Canadian Forest Fire Emissions Prediction System (CFFEPS), used by GFFEPS.
Historical input data (parallelograms) are shown in blue. Current input data (parallelograms) and operational
calculations (rectangles) are shown in green. Predictive models (rectangles) are shown in red (CFFDRS), purple
125 **(CFFEPS) and orange (burned area mapping). Units reflect those used in the text. The plume rise module and**
the emissions vertical distribution are not discussed in this paper.

2.1 The Canadian Forest Fire Danger Rating System

The Canadian Forest Fire Danger Rating System (CFFDRS) has been an important part of forest protection operations
in Canada since 1970 (Stocks et al., 1989). The two principal models of the CFFDRS are the Canadian Forest Fire Weather
130 Index (FWI) System, which models fuel moisture and potential fire behaviour in the forest, and the Canadian Forest Fire

Behaviour Prediction (FBP) System, which predicts physical fire behaviour in specific vegetative landscapes, referred to as fuel types.

The Canadian Forest Fire Weather Index (FWI) System (Van Wagner 1987) is a set of numerical codes and indices rating relative fire potential. Built on measurements from jack pine forests near Petawawa ON, the system is strictly weather dependent and independent of forest fuel type. Daily and hourly temperature, humidity, wind speed and precipitation are used to estimate the various FWI system indices. The FWI System consists of six components that account for the effects of weather on fuel moisture and potential fire behaviour. The first three components are the fuel moisture codes. These include the Fine Fuel Moisture Code (*FFMC*), the Duff Moisture Code (*DMC*) and the Drought Code (*DC*). These are numeric ratings, or indices, of the moisture content of the litter and other fine fuels, of the loosely compacted organic layers of moderate depth, and of the deep, compact organic layers respectively. Their values rise as moisture content decreases. The remaining three components – the Initial Spread Index (*ISI*), the Buildup Index (*BUI*) and the Fire Weather Index (*FWI*) – are fire indices. These indices represent respectively the rate of fire spread, the fuel available for combustion, and the frontal fire intensity; their values rise as the fire danger increases.

The FWI system is internationally-recognized and is used by several countries including Canada, certain US states, Mexico, ASEAN nations, New Zealand and a number of European nations (Taylor and Alexander, 2006). Daily maps in near-real time are routinely generated and displayed on the Canadian Wildland Fire Information System (https://cwfis.cfs.nrcan.gc.ca/home, last accessed 2023-12-05; Lee et al., 2002), the European Fire Information System (https://effis.jrc.ec.europa.eu/, last accessed 2023-12-05; Vitolo et al., 2020) and the Global Wildfire Information System (https://gwis.jrc.ec.europa.eu/ , last accessed 2024-01-24).

The Canadian Forest Fire Behaviour Predictions (FBP) System (Forestry Canada Fire Danger Group 1992; Wotton et al., 2009) is an extension of the FWI system. It captures the physical measures of fire behaviour within certain Canadian landscapes. The FBP system consists of a series of empirical models that predict fire behaviour conditions for 18 common fuel types in Canada (see Table 1). Using daily and hourly weather values and indices from the FWI system as inputs, the FBP system predicts for the prescribed fuel types in Canada measurable physical variables including the forward rate of spread (*ROS*) in m min^{-1}, head fire intensity (*HFI*) in kW m^{-1}, surface, crown and total fuel consumptions (*SFC*, *CFC*, *TFC*) in kg m^{-2} (where *TFC* = *SFC* + *CFC*) and crown fraction burned (*CFB*) as a fraction or percentage. It is worth noting that the FBP system was designed with a focus on the most hazardous fuels in Canada and under high fire behaviour conditions. Challenges will be present adapting FBP to broader, global landscapes and addressed in the methodology.

The fuel consumption values (*SFC*, *CFC*, *TFC*) predicted by FBP system are central to the wildfire emissions predictions in CFFEPS and in GFFEPS. It is assumed that the fuel consumed by the fire translates directly to emissions, and that components of tracer emissions, that in turn are injected into the atmosphere, directly contribute to wildfire smoke (i.e., one tonne of fuel consumed becomes one tonne of smoke emissions, including ash and soot). In forecast model applications, FWI values can be calculated daily and hourly with outputs from numerical weather models, and tracer emissions can be calculated in near-real time for fire locations as they are identified.

165

Table 1. Canadian Forest Fire Behavior Prediction (FBP) System fuel types.

Group/Identifier	Descriptive name
Coniferous	
C-1	Spruce-lichen woodland
C-2	Boreal spruce
C-3	Mature jack or lodgepole pine
C-4	Immature jack or lodgepole pine
C-5	Red and white pine
C-6	Conifer plantation
C-7	Ponderosa pine - Douglas-fir
Deciduous	
D-1	Leafless aspen
D-2	Aspen - green
Mixedwood	
M-1	Boreal mixedwood - leafless
M-2	Boreal mixedwood - green
M-3	Dead balsam fire mixedwood - leafless
M-4	Dead balsam fire mixedwood - green
Slash	
S-1	Jack or lodgepole pine slash
S-2	White spruce-balsam slash
S-3	Coastal cedar - hemlock - Douglas-fir slash
Open	
O-1a	Matted grass
O-1b	Standing grass

2.2 The Canadian Forest Fire Emissions Prediction System

GFFEPS follows the same general methodology as its predecessor CFFEPS, which has been documented in recent
170 publications (Makar et al., 2020, Chen et al., 2019). CFFEPS uses fire weather conditions modelled by the FWI system and
fire behaviour by the FBP system to determine fuel consumed per unit area. Burned area (per day) in CFFEPS is based on
annual ecoregion and vegetation-specific burned-area climatology normalized by the number of satellite-detected hotspots

(Chen et al., 2019). For CFFEPS, values of historical average burned area per hotspot (i.e., burn-area climatology for 10 years from 2012-2021) were calculated by each fuel type and ecoregion for each province/territory, by relating recorded hotspots to

175 annual burned area statistics as reported by provincial and territorial agencies (the National Burned Area Composite (NBAC): https://cwfis.cfs.nrcan.gc.ca/datamart/download/nbac, last accessed 2023-12-04).

The application of CFFEPS calculations is conducted on each satellite-detected hotspot. Fire weather conditions are interpolated to the hotspot location and fire behaviour is calculated based on the fuel type sampled at the hotspot location. Burned area per day, based on the burned-area climatology, is used and persistence of burned-area rate is assumed for the

180 ensuing 24-hour forecast period.

While CFFEPS has been demonstrated to be an excellent means of wildfire emission estimate for air-quality forecast application within a North American context, several critical issues arise when expanding its utility to the global scale. These include expanding the FWI calculations to a global domain, establishing a global fuels map compatible with the FBP system, and determining the most relevant, compatible fuel type and fuel consumption equations within the CFFDRS framework to

185 represent global landscapes.

2.3 Global Models

There are several published global fire-emissions models (Pan et al., 2020). For this study we included

- Global Fire Assessment System (GFAS1.2, Kaiser et al., 2012),
- Global Fire Emissions Database (GFED4.1s, van der Werf et al., 2017),
190 - Fire Inventory from NCAR (FINN 1.5/2.5, Wiedinmyer et al., 2011, Wiedinmyer et al., 2023).

The GFED and FINN models use the bottom-up approach and estimate effective fuel consumption rate E (mass of fuel consumed per unit area per time – kg m^{-2} d^{-1} or tonnes ha^{-1} d^{-1}) based on the equation of Seiler and Crutzen (1980):

$$E = BA \times FL \times CC \times EF \tag{1}$$

where burned area (BA) is a measure of the spatial extent of fire activity over a period of time (ha d^{-1}), fuel load (FL) is the

195 biomass of combustible fuels (t ha^{-1}) on the landscape, and combustion completeness (CC) is the percentage of the total available biomass consumed by fire (%). For final emission rates related to chemical component emissions such as CO, CH$_4$ and particulate matter, the effective fuel consumed (BA x FL x CC) is multiplied by species-specific emission factors (EF) in g of emissions per kg of dry fuel consumed. These factors are typically derived from field or laboratory measurements and can be specific to fuel type and burn conditions as measured by combustion efficiency (Urbanski 2014, Chen et al., 2019).

200 Expanding CFFEPS into the global domain, GFFEPS follows a similar methodology to GFED and FINN. An adjusted version of Eq. (1) is used in GFFEPS as the FL x CC term is replaced by the total fuel consumption (TFC) of the Canadian Forest Fire Behaviour Prediction (FBP) system. In doing so, daily fire behaviour is captured by using the FWI and FBP systems; we replace the static combustion completeness used by standard bottom-up models such as GFED and FINN with more dynamic parameterizations contained within the CFFDRS framework.

205   The global regions commonly used in global fire-emissions analyses are shown in Fig. 2 and described in Table 2.

AUST	Australia	MIDE	Middle East
BOAS	Boreal Asia	NHAF	Northern Hemisphere Africa
BONA	Boreal North America	NHSA	Northern Hemisphere South America
CEAM	Central America	SEAS	Southeast Asia
CEAS	Central Asia	SHAF	Southern Hemisphere Africa
EQAS	Equatorial Asia	SHSA	Southern Hemisphere South America
EURO	Europe	TENA	Temperate North America
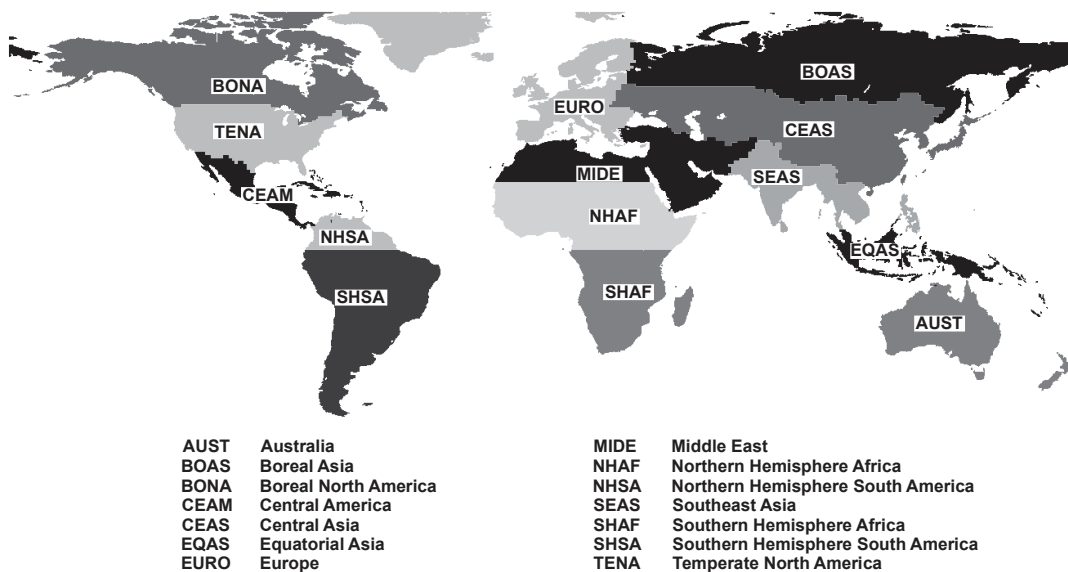
Figure 2. Global regions used in this study following those defined in Giglio et al. (2006). See Table 2 for complete
210   **description.**

Table 2. Global regions used in this study following those defined in Giglio et al. (2006).

Abbreviation	Region	Description
BONA	Boreal North America	Alaska and Canada
TENA	Temperate North America	Continuous United States
CEAM	Central America	Mexico and Central America
NHSA	Northern hemisphere South America	South America north of the Equator
SHSA	Southern hemisphere South America	South America south of the Equator
EURO	Europe	Europe including Baltic states, excluding Belarus and Ukraine
MIDE	Middle East	Africa north of tropic of Cancer, the Middle East and Afghanistan
NHAF	Northern hemisphere Africa	Africa between the Tropic of Cancer and the Equator

SHAF	Southern hemisphere Africa	Africa south of the Equator
BOAS	Boreal Asia	Russia north of 55°N
CEAS	Central Asia	China, Mongolia, Russia south of 55°N, former Central Asian USSR
SEAS	Southeast Asia	Pakistan, India and Indochina
EQAS	Equatorial Asia	Malaysia, Indonesia and Papua New Guinea
AUST	Australia	Australia and New Zealand

3 Data

To calculate global fire emissions, critical input data are needed. These include global land classifications, satellite-detected fire locations (a.k.a. hotspots), daily global weather and agricultural burning statistics.

3.1 Land Classification

A land classification system is required to link tree species and landscapes at fire locations to fire behaviour, fuel consumption and emissions as predicted by FBP. Global climate models use a variety of vegetation classification systems. The Global Land Cover 2000 Project by European Commission (GLC2000, Bartholome and Belward, 2005) is such a product (Fig. 3 and Table 3) and was adopted in the development of this initial version of GFFEPS. Developed in collaboration with a network of partners around the world, the general objective of GLC2000 was to provide a harmonized land-cover database over the whole globe for the year 2000. The year 2000 was selected as a reference year for environmental assessment in relation to various activities. While other land use databases are available (e.g., MODIS, etc.), GLC2000 was selected for its global spatial resolution with 1-km at the equator, for its level of detail in the number of land use types, for ease of data usage, accessibility and for consistency throughout our analysis. However, we note that the same methodology developed here using GLC2000 may be used with other land-use databases.
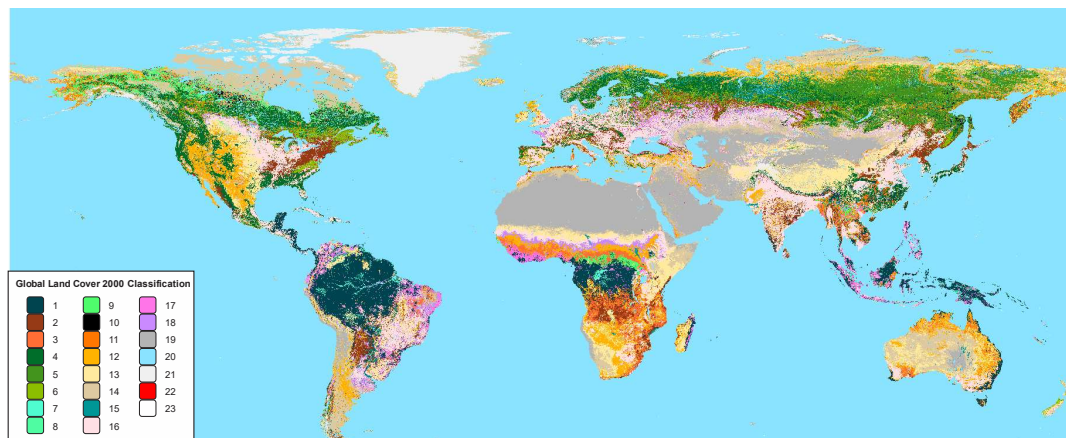
Figure 3. Global Land Cover 2000 classification. See Table 3 for land classification descriptions for numbered values appearing in the legend.

230

Table 3. Global Land Classification 2000 (GLC 2000) codes and descriptions.

GCL 2000	Description
1	Tree Cover, broadleaved, evergreen
2	Tree Cover, broadleaved, deciduous, closed
3	Tree Cover, broadleaved, deciduous, open
4	Tree Cover, needle-leaved, evergreen
5	Tree Cover, needle-leaved, deciduous
6	Tree Cover, mixed leaf type
7	Tree Cover, regularly flooded, freshwater (& brackish)
8	Tree Cover, regularly flooded, saline water
9	Mosaic: Tree cover / Other natural vegetation
10	Tree Cover, burnt
11	Shrub Cover, closed-open, evergreen
12	Shrub Cover, closed-open, deciduous
13	Herbaceous Cover, closed-open
14	Sparse Herbaceous or sparse Shrub Cover
15	Regularly flooded Shrub and/or Herbaceous Cover
16	Cultivated and managed areas
17	Mosaic: Cropland / Tree Cover / Other natural vegetation

18	Mosaic: Cropland / Shrub or Grass Cover
19	Bare Areas
20	Water Bodies (natural & artificial)
21	Snow and Ice (natural & artificial)
22	Artificial surfaces and associated areas
23	No data

A review of regional descriptions of each land classification provided a means to assign FBP fuel types to all GLC2000 classifications present in each region based on expert opinions. The assigned fuel for specific classifications may vary between regions and confidence in assignments varies. The resulting mapped FBP fuel types are shown in Fig. 4.
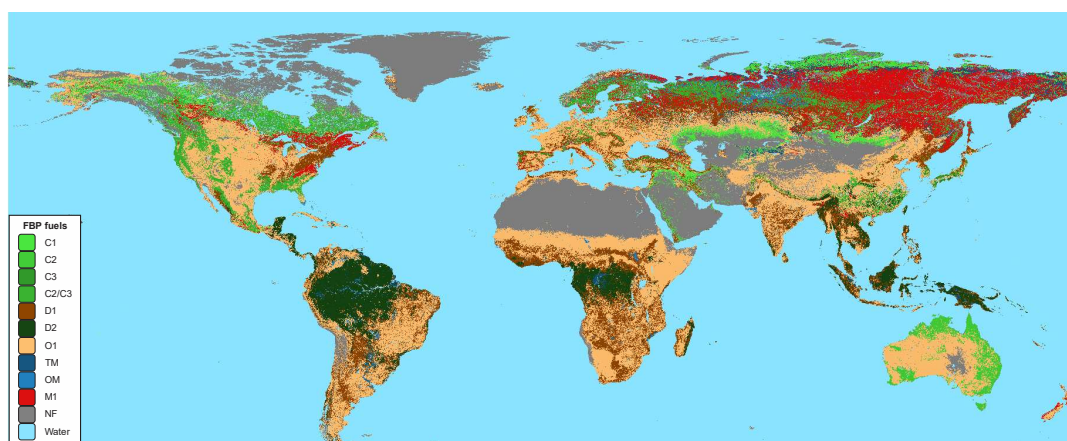
Figure 4. Canadian Forest Fire Behaviour Prediction (FBP) System fuel types as assigned from the Global Land Classification 2000. See Table 1 for descriptions of FBP fuel types appearing in the legend. TM and OM, not listed in Table 1, represent treed and open muskeg.

Certain GLC2000 land cover classifications, such as peat lands (described as "regularly flooded"), do not have any corresponding fuel types in FBP. Methods for representing these are discussed in the supplemental information section. Also, GLC2000 land classifications 16, 17 and 18 were assigned to agriculture regions and treated separately. The resulting map (Fig. 5) presents the supplemental fuel types, which take precedence over the FBP fuel types where they occur.
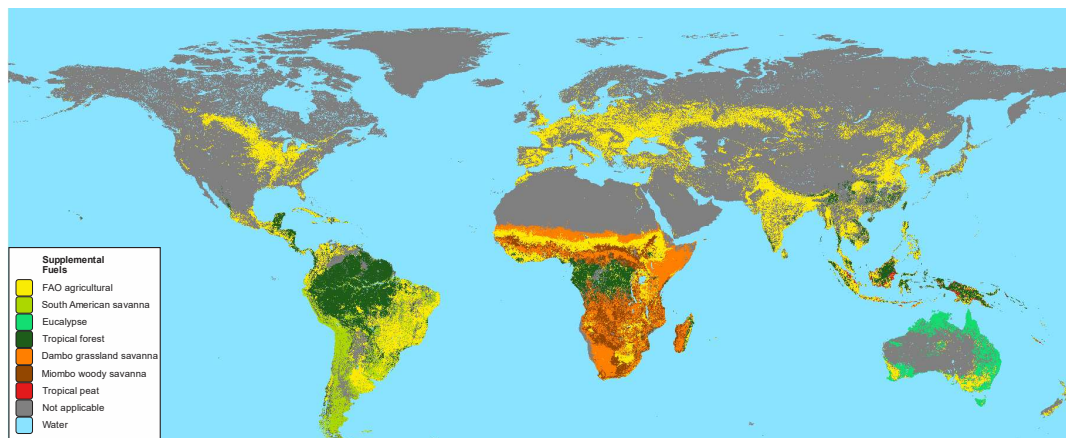
Figure 5. Supplemental fuels as described in the supplemental information section. Note that these fuels take precedence over the FBP fuel types presented in Fig. 4.

In addition to the land-cover classification, GFFEPS requires surface fuel load, forest floor depth and bulk density data (https://www.ciffc.ca/publications/glossary, last accessed 2024-01-24) for FBP system calculations (derivation of these data are discussed later in the methodology section). As part of the GFED3.x and 4.x wildfire emissions model, van Leeuwen et al. (2014) and van der Werf et al. (2017) collected detailed fuel load and consumption data from 201 and 591 sites respectively through literature reviews. However, the biomes used by GFED do not directly correspond to land classifications in the GLC2000; therefore, the biomes of these sites were matched to GLC2000 land classifications, with varying degrees of confidence depending on the number of sites within biome and the consistency of correspondence between biome and GLC2000 land use classifications. Given the matches, fuel load values were then applied (see supplemental information).

3.2 Satellite Hotspots

GFFEPS requires the times and locations of active fires. Similar to most global fire emission models, these are obtained in the form of hotspots identified from infrared satellite imagery. GFFEPS uses hotspots detected by the Visible Infrared Imaging Radiometer Suite (VIIRS) sensor and obtained from the Fire Information for Resource Management System (FIRMS) provided by NASA and the U.S. Forest Service. The VIIRS sensor was first launched on board the Suomi National Polar-Orbiting Partnership (S-NPP) satellite in 2011 (also onboard NOAA-20, NOAA-21 satellites since 2017 and 2022, respectively) and provides coverage of every location on the globe at least twice daily, with higher frequency at high latitudes. Not all fires are detected; some are too small, some are short-lived and burn between satellite overpasses, and some burn under thick cloud cover or heavy smoke that render them invisible. In spite of these limitations, hotspot data from VIIRS provides a picture of global fire activity that is consistent, continuous, and sufficiently complete.

270   Hotspot data from other sensors is available from FIRMS as well, including the Moderate Resolution Imaging Spectroradiometer (MODIS) and the Advanced Baseline Imager (ABI). VIIRS was selected because of its higher resolution (375m, compared with 1 km for MODIS and 2+ km, depending on latitude, for ABI) but in the future, data from other sensors could be incorporated as inputs to GFFEPS. Unlike other top-down approaches that use quantitative FRE/FRP to parameterize fuel consumption, GFFEPS does not use satellite sensor quantitative measurement; instead, only high-resolution hotspot

275   location and ignition timing is required. This allows potential future expansion of GFFEPS to use other remote sensing data, including radiometric measurements such as Interferometric Synthetic Aperture Radar (InSAR) with the advantage of detecting fire through cloud and smoke at high spatial resolution (Ban et al., 2020; Goodenough et al., 2014).

3.3 Global Weather

        Global weather conditions, essential in calculating FWI, are calculated with ECCC's Global Environmental Multiscale

280   model. GEM is the core numerical weather prediction (NWP) model of ECCC's operational weather prediction services. Global scale GEM currently provides gridded meteorological conditions at 15-km resolution every 3-hour time steps to calculate fire behaviour conditions and smoke emissions in GFFEPS. Extracted surface variables include windspeed, relative humidity, temperature and 24-hour accumulated precipitation to calculate FWI; additional variables including vapour pressure deficit, solar day length etc. were extracted for FBP.

285   Environment and Climate Change Canada now has FWI calculations incorporated as part of model product processes in regional weather forecasts. Figure 6 shows a sample global map of daily value of the Buildup Index (BUI) predicted for the reported hotspots for September 1, 2019.
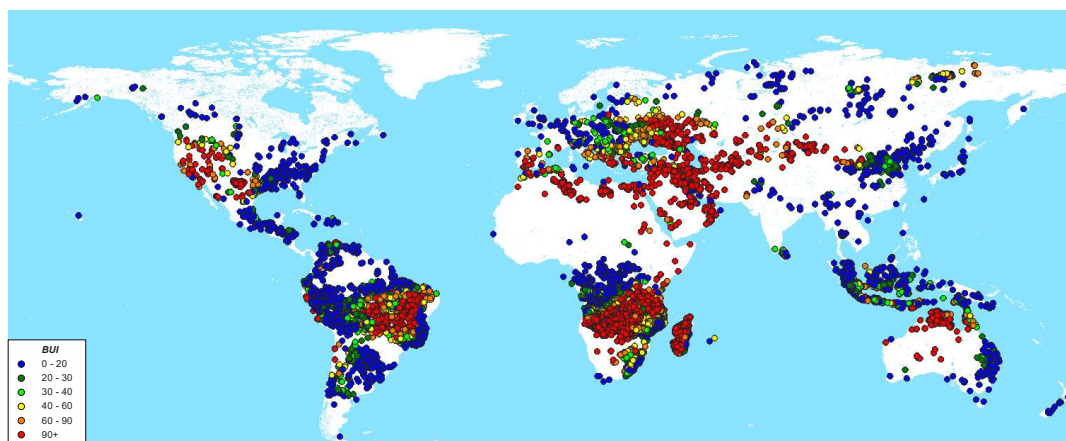
Figure 6. Buildup Index (BUI) for September 1, 2019 as interpolated to the 63,566 hotspot locations observed on
290   **that date. The BUI is calculated using meteorological data from Environment and Climate Change Canada's**
        Global Environmental Multiscale (GEM) model.

3.3.1 Growing Season Index

Deciduous leaf-out (greenness), and grass dormancy (curing), are important factors in fire behaviour. The FWI system does not have a built-in method to predict these phenologies; instead, the FBP system relies on users to provide both grass
295 curing fraction as well as the leaf-out status of deciduous vegetation based on physical observations. To address this in GFFEPS, the Growing Season Index (*GSI*) by Jolly et al. (2005) was used as a surrogate to capture the seasonal dynamics of deciduous leaf-out. This model uses simple threshold functions (zero below a minimum value, one above a maximum value and a linear relation from 0 and 1 between the minimum and maximum values; reversed in the case of vapour pressure deficit) based on the following three observable parameters:

300   •   minimum temperature (linear response range between -2°C and 5°C),

    •   vapour pressure deficit (linear response range between 900 Pa and 4100 Pa),

    •   hours of daylight (linear response range between 10 hrs and 11 hrs).

A daily *GSI* is calculated as the product of these three output values; afterwards, a moving average over the previous 21-days' *GSI* values is applied to reduce abrupt daily variability thus better mimicking plant response (Jolly et al., 2005).
305 Figure 7 shows a sample global map of daily value of the *GSI* predicted for the reported hotspots for September 1, 2019.
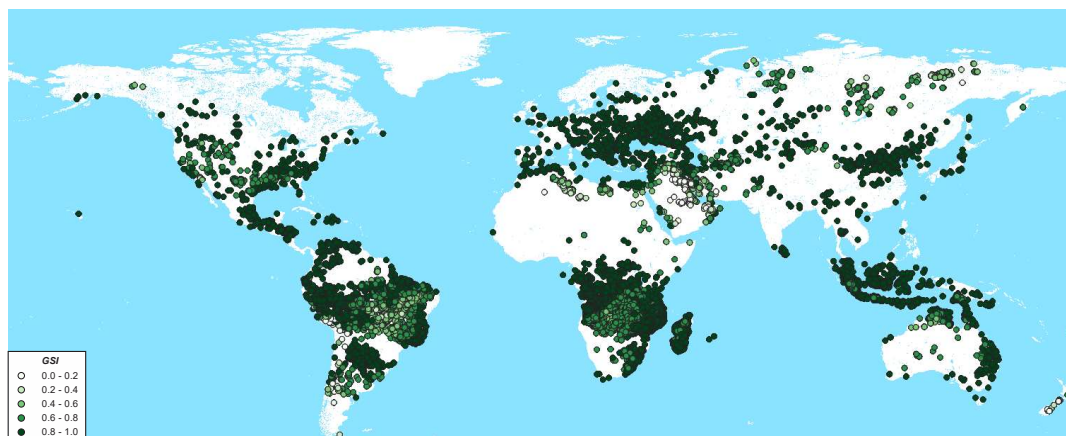
Figure 7. Growing Season Index (*GSI*) for September 1, 2019 as interpolated to the 63,566 hotspot locations observed on that date. The 21-day average *GSI* is calculated using meteorological data from Environment and
310 **Climate Change Canada's Global Environmental Multiscale (GEM) model.**

The *GSI* is a surrogate for the greenness of the Normalized Difference Vegetation Index (NDVI; Pettorelli, 2013), typically measured via remote-sensing approaches. *GSI* provides a continuous calculation of the greenness value, both

spatially and temporally, while NDVI must be stitched together from satellite data. Regardless, in the future, observed NDVI
315   could be assimilated and replace *GSI* calculations for grass curing and deciduous green-up.

3.3.2 Foliar Moisture Content

The Foliar Moisture Content (*FMC*) is another phenology required by the FBP system, and is defined as the moisture
content of live needles in a conifer tree (Alexander, 2010a). On average, the *FMC* of coniferous trees is 120% during the fire
season in Canada, but in the spring as the ground thaws, the *FMC* dips to 85%, reflecting a decrease as the foliage transpires
320   while the roots are still frozen. This spring dip of *FMC* increases the likelihood of crown fire initiation in conifer trees (fires
rarely crown in deciduous trees); in turn, this affects crown fuel consumption (*CFC*) and thus emissions into the atmosphere.
The Julian date of the minimum *FMC* is denoted as D_o.

The CFFDRS has a means of calculating the *FMC*, yet this is only valid in North America. To expand this to a global
domain, a new set of equations was developed to calculate *FMC* in Eurasia following the principles of the original approach.
325   As the spring dip in the *FMC* value is based on the assumption that the ground is frozen in the winter, *FMC* calculations are
limited to northern latitudes where D_o exceeds 90 (i.e., minimal *FMC* occurs on or after March 31); elsewhere, the default
FMC value of 120% is used in the northern hemisphere In the southern hemisphere, a default *FMC* value of 147% is used
year-round, as used in New Zealand (Pearce et al., 2008; Alexander, 2010a), where coniferous trees rarely reach freezing
conditions .

330   The *FMC* used in the CFFDRS was based on observations from eight stations in Canada (Forestry Canada Fire Danger
Group 1992). The assumption was that dates of minimum *FMC, D_o*, followed climatological isotherms with elevation
adjustments of 0.026 days m^{-1}. Following the same rationale, climatological maps of isotherms for March, April and May
were collected for Eurasia. Assuming a parabolic shape for the April 0°C isotherm, and setting the point of minimum latitude
at 47°N and 120°E along the isotherm with a second point at 65°N and 30°E to define the curve, the resulting equation for the
335   latitude-longitude contour of the date of the minimum FMC becomes

$$LATZ \ = \ (65-47)/(30-120)^2 \times (LON-120)^2 \ + \ 47 \ = \ 0.0022 \times (LON-120)^2 \ + \ 47. \qquad (2)$$

The resulting curve corresponds to D_o, the contour of the Julian day of minimum *FMC*, chosen as 151. In Canada, D_o
drops off at approximately 2 days per degree latitude so in Asia,

$$D_o \ = \ 151 \ + \ 2.286 \ * \ (LAT - LATZ). \qquad (3)$$

340   Using 146°W and 12°W as the lines dividing Eurasia from North America, D_o can be calculated for the northern
hemisphere (not required for the southern hemisphere as noted above). Figure 8 illustrates the global map of the month when
the day of minimum *FMC* (D_o) occurs.
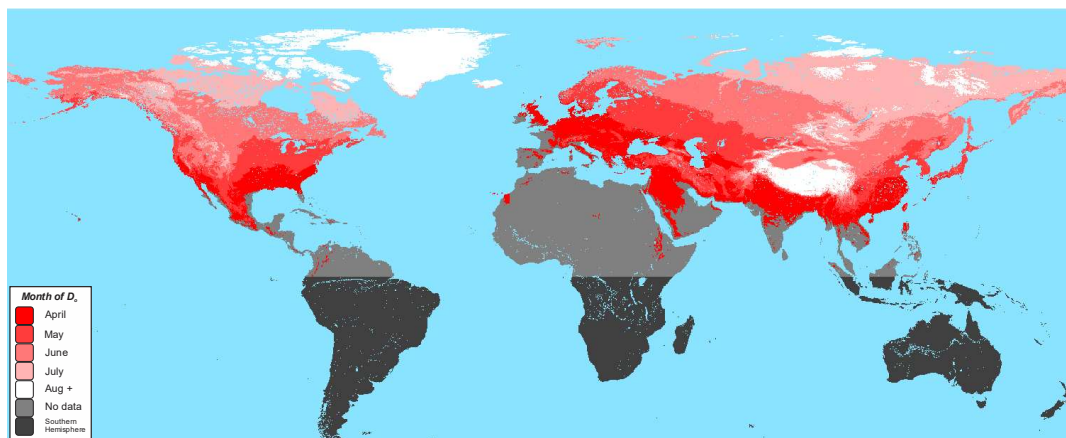
Figure 8. Month of occurrence of the day of minimum Foliar Moisture Content Content (D_o), when the *FMC*
345   **dips to 85% from 120%. The no data zone and the southern hemisphere are assumed to have no spring dip and**
thus *FMC* values are set to a constant 120% and 147% respectively.

3.4 Agricultural Burning

Agricultural burning is governed by a variety of processes that differ from those encompassed by Eq. (1). These must
350   be addressed separately in order to properly model the contribution of the agricultural sector to global fire emissions.
Croplands cover 12% of the ice-free land surface. It is estimated that residue burning accounts for 5% of global emissions
(Cassou, 2018; Bond et al., 2013). Depending on the time of year, farmers may burn the residue after harvest. There are a wide
variety of crops but the three principal crops whose post-harvest residues are typically burned are maize, rice and wheat.
Pouliot et al. (2017) provided fuel loads for these and several other crop residues in the USA. These are as much as twice the
355   default fuel load of the FBP system's standing grass FBP O-1 (0.35 kg m^{-2}), indicating the need to differentiate agricultural
burning from grass fuel.

In order to include these effects into GFFEPS, agricultural burning calculations were applied to GLC2000 land
classifications 16, 17 and 18 (see Fig. 3 and Table 3). Streets et al. (2003) presented the following equation to estimate the
total mass of crop residue burned in the field (R) as

360     $$R = P \times N \times D \times B \times F \tag{4}$$

where

- P = crop production;
- N = crop-specific production-to-residue ratio;
- D = dry-matter-to-crop ratio;

365   • B = the percentage of dry matter residues that are burned in the field;

         • F = the crop-specific burn efficiency ratio.

The first four terms in Eq. (4) are provided in data collected by the United Nations' Food and Agriculture Organization (FAO). The FAO collects global agricultural production, presenting national amounts on their FAOSTAT page (https://www.fao.org/faostat/en/#data/GB; last accessed 2023-12-13). This page provides past crop residue burning values

370   by nation per year. This value, E_{FAO}, captures dry weight of crop production (P), crop-specific production-to-residue ratio (N), dry-matter-to-crop ratio (D) and percentage of dry matter residues that are burned in the field (B) as a single value, simplifying the application of Eq. (4) to

$$R = (P \times N \times D \times B) \times F = E_{FAO} \times F. \qquad (5)$$

Values for burning efficiencies (F) for specific crops were then taken from Turn et al. (1997).

375   Annual statistics of biomass burned (dry matter) from the FAOSTAT were compiled for each country for the years 2012, 2015, 2018, 2019 and 2020. Similarly, the number of VIIRS hotspots occurring within the GLC2000 land classifications assigned to agricultural burning were counted for each country for the same years. National statistics were then grouped according to regions outlined by Giglio et al. (2006, see Table 3). From this, average emissions per agricultural hotspot were calculated, which were then used in subsequent GFFEPS estimates of emissions from agricultural burning. The temporal

380   behaviour of agricultural fires was based on a modified diurnal curve for agricultural burning approximating a Gaussian curve centered on 15:00 LST (Eyth et al., 2022, McCarty et al., 2009).

We note that this approach is a significant departure from the method used in other global fire emission models. Agricultural burning is typically conducted at small scales and short durations and, as a result, are difficult to detect with satellite-based remote sensing. GFED4.1s simulates these undetected agricultural fire emissions by extrapolating the

385   agriculture areas burned detected by remote sensing (Randerson et al., 2012, van der Werf et al., 2017). The approach used by GFFEPS avoids the small fire detection issue associated with agricultural burning by using country-specific report data from FAO, while assuming small fires in other, non-agricultural, landscapes were deemed inconsequential. In principle, the data and methodology outlined for GFFEPS captures all crops burned, regardless of fire size, statistically accounted for and reported by individual countries. With that said, the Tier 1 methodology used by the FAO to determine this value may not be

390   rigorous in developing countries (Tubiello et al., 2014); nevertheless, its application in GFFEPS seemed a direct and practical solution to the small fire issue specific to agriculture activities.

4 Methodology

The methodology of CFFEPS is documented in Chen et al. (2019). GFFEPS follows the same methodology as CFFEPS but uses additional data sets and alterations described in this section. Likewise, GFFEPS follows Eq. (1) and the sections

395   described here under the methodology follow each of the equation variables. Global fire emissions produced by GFFEPS were

first examined for interannual and interregional variability, then a multi-model comparison was conducted between GFFEPS and four other published wildfire emissions models to test its general performance.

4.1 Burned Area

400 GFFEPS requires an estimate of burned area (*BA*) for each hotspot. Historical data for 2012-2019 was obtained from the MODIS burned area product (Giglio et al., 2016), which provides gridded monthly burned area for the globe. Total *BA* and hotspot count were determined for each combination of region (Fig. 2 and Table 2), month, and land-cover type (Fig. 3 and Table 3).

Dividing total *BA* by number of hotspots provides a simple estimate of burned area per hotspot. However, in some cases hotspots were found in the same location two or more days in a row, or within a short period of time. This could represent a

405 pixel partially or incompletely burned, as would be the case if a fire was moving slowly, or burning in episodes separated by smouldering. In other cases, hotspots were occurring in a location repeatedly for several months or even years, indicating a non-fire heat source, usually an industrial facility. Whatever the underlying reason, it was decided that these hotspots should not be assigned the same burned area as lone or isolated hotspots.

For each hotspot, the number of times burned, *T*, was calculated as the number of hotspots that occurred in the last 6

410 months within the VIIRS I-band pixel (375m) centered on that hotspot. As the current hotspot was included in the count, *T* was always at least 1. The 6-month time frame reflects our assessment that a completely burned vegetation is unlikely to regrow quickly enough to be susceptible to fire again within that time.

Total burned area and the sum of $1/T$ were derived for each combination of month, region and land-cover type to derive a burned area estimate for lone hotspots:

415 $$E_L = BA / \sum_j (1/T_j) \qquad (6)$$

where E_L is the area-burned estimate for single (lone) hotspots, *BA* is the total burned area, and T_j is the times burned metric and *j* is the hotspot number. Note that for repeatedly burned pixels, the use of Eq. (6) prevents their burned area, and consequently their emissions, from being overestimated.

For region-month-landcover combinations with fewer than 1000 hotspots, the resulting E_L values were not statistically

420 significant; in this case, a larger dataset region-month combinations were used instead, combining all the land-cover types together within a region and month.

In subsequent emissions calculations, the number of times burned is similarly calculated. Area estimates for lone hotspots ($T = 1$) were set equal to E_L. For hotspots in previously burned pixels, the burned area estimate was set to E_L divided by the times burned metric:

425 $$E = E_L / T \qquad (7)$$

This method reduces the burned area in multiple-hotspot locations, preventing the same fuel from being burned multiple times during emissions calculations. Hotspots generated by industrial heat sources remain in the dataset, but they are assigned a very small burned area; as a result, their impact on emissions estimates is minimized.

4.2 Fuel Load

430   The fuel loads (*FL*) used in GFFEPS are based on values collected from the literature review by van Leeuwen et al. (2014) and from van der Werf et al. (2017) as used in GFED. From these data, fuel load values were assigned to surface, crown and grass fuel loads (*SFL*, *CFL*, *GFL*) and averaged across sites with a common GLC2000 land classification. The source data had fields ranging from simple totals to very specific fuel component descriptions per site. When this ancillary data was available, certain heavier fuels were excluded from fuel loads, such as live stems and branches with diameters greater

435   than 10 cm, and were deemed inflammable (as residual snags).

        Following this initial classification, attention was given to regional differences, many of which are summarized in the supplemental section, especially for high-emitting regional land classifications. These include boreal forests, tropical forests, tropical peat, wooded and open savanna grasslands, and Australian eucalypt forests.

4.3 Combustion Completeness

440   The combustion completeness (*CC*) used in GFFEPS is based on the total fuel consumption (*TFC*) as calculated by FBP. The forecasted weather and FWI described earlier are combined with the FBP fuel types as derived from the GLC2000 land classification to provide the necessary inputs for the FBP calculations.

        Implementing CFFEPS globally, adjustments to the original FBP fuel loads and fuel consumption equations were necessary. The FBP system was designed specifically for Canadian fuel types (Table 1). Extrapolating these to a global

445   environment for fuels outside Canada was necessary. In this process, a few critical limitations in the Canadian-specific FBP system were also recognized and addressed, specifically:

- Surface fuel loads (*SFL*) were used to adjust the surface fuel consumption (*SFC*) equations within FBP; replacing the 1.5 and 5.0 kg m^{-2} present in most fuel consumption equations.
- Grass fuel consumption (*GFC*) was separated from surface fuel consumption (*SFC*); along with crown fuel

450   consumption (*CFC*), expressing a new total fuel consumption (*TFC*):

$$TFC = GFC + SFC + CFC. \tag{8}$$

    Grass fuel consumption was adjusted to account for the degree of curing, the process by which grass dries over the season, by multiplying the grass fuel load by the grass curing adjustment factor (*C*):

$$GFC = C * GFL. \tag{9}$$

455   - Grass curing adjustment factor was based on the equation derived for dormant grass in savanna grasslands using drought code (*DC*) values (see Appendix A.3):

$$C = 100\% \times (1 - e^{-0.0027\,DC}). \tag{10}$$

- Green-up (leaf-out) of deciduous forests (FBP fuel type D-1 and D-2, Table 1), normally a dichotomous process in FBP (Alexander, 2010b), was set to a fractional scale and using this the surface fuel consumption (*SFC*) of green

460   deciduous (D-2) was derived by adjusting the surface fuel consumption for FBP class of "leafless deciduous" (D-1) by (1 - *GSI*):

$$SFC(\text{D-2}) = (1 - GSI) \times SFC(\text{D-1}). \tag{11}$$

4.3.1 Peat Fires

Fires in equatorial Asia (Indonesia, Malaysia and New Guinea) in GLC2000 land classifications 7, 8, 9, 11 and 14 (see
465   Table 2) were assumed to be peat fires, which require special consideration. Field et al. (2004) determined that most severe haze events from peat fire smoke in Indonesia occurred at a Drought Code (*DC*) value of 388.2 and higher. They accordingly assigned boundaries between moderate-high and high-extreme categories at *DC* values of 264.4 and 346.9. Based on these values, a logistic equation was constructed to mimic these conditions

$$SFC = 105.6/\left[1 + e^{-0.1(DC-3\ .2)}\right] \tag{12}$$

470   where 105.6 kg m^{-2} reflects the fuel load of the tropical peatland fuels (van Leeuwen et al., 2014). A detailed description of this derivation is provided in the supplemental section.

Outside of equatorial Asia, boreal peatlands were assessed as treed (shaded, enclosed) or open peat lands, based on, respectively, the "Tree Cover, regularly flooded, freshwater" or "Regularly flooded Shrub and/or Herbaceous Cover" descriptions in the GLC2000 land classification (Table 3). Depending on current FWI conditions, a treed peatlands fuel type
475   is assigned to boreal mixedwood forest with 50% conifer trees (fuel type M-1/2) when the *DC* is above 330, and to fuel type D-2 at lower *DC* values; open peatlands are assigned a non-fuel type until the *DC* reaches 650, at which point they assumed to burn as fully cured standing grass (O-1b). These thresholds are prescribed following earlier study of Thompson et al. (2019).

4.3.2 Eucalypt

Over 22% of Australia is forested, of which 78% is eucalypt, also known as jarrah (Sullivan et al., 2012). Eucalypt
480   does not fit any fire behaviour reflected in the FBP system so an effort was made to create a fuel consumption model specific to eucalypt from the published literature (Hollis et al., 2010). A sigmoidal fuel consumption curve was developed similar in structure to those used in the FBP System (Appendix A.5). An upper limit of 90% was used as it was assumed that standing snags would likely be left after a fire-front passage.

$$TFC = 90\% \times [1 - e^{(0.01976\,BUI)}]^3 \tag{13}$$

485   Additionally, Oliveira et al. (2015) examined fire activity in tropical savannas in northern Australia. They described the landscapes as open woodlands, woodlands and open forests with forest protective covers of <10%, 10-30% and 30-70% respectively. Average values of these fractions were used in GFFEPS, with the balance as grass fuels. A detailed description of this derivation is provided in the supplemental section.

4.4 Emissions Factors

490 For emission factors per chemical species (*EF*), GFFEPS follows the same approach as CFFEPS (Chen et al., 2019). Combustion is divided into three classes based on the crown, surface and grass fuel consumptions. Surface fuel is further divided into litter (0-1.2 cm), upper (1.2-7 cm) and lower (7-18 cm) duff layers following fuel-based depths and fuel-dependent bulk densities (mass of fuel per unit volume in g cm^{-3}, Anderson, 2000; https://www.ciffc.ca/publications/glossary, last accessed 2024-01-24). The fuel consumed in each layer is burned in succession through flaming, smoldering and residual

495 combustion stages, which are then convolved over time. Emission rates per chemical species emitted are defined through each stage of combustion by combining emission factors for flaming, smoldering, and residual with FBP's *CFC*, *SFC* model values. By modelling the total fuel consumption (kg m^{-2}), emissions per species are calculated based on species emission factors (g kg^{-1}) as defined in Chen et al. (2019).

In the current initial application of GFFEPS, for direct assessment of fuel consumption values, and comparison with

500 other global fire emissions inventory, a simple unit emission factor is first presented for estimating smoke emissions, followed by an application of standard emission factor of 500 g kg^{-1} for estimating total carbon emissions (Thomas and Martin, 2012).

5 Results

The GFFEPS model was run for six consecutive years (2015 to 2020) to examine the quantitative fire emissions globally for each year, and interannual variability predicted by the model. Model output was measured in total smoke emissions

505 released from fires. This equals the total fuel consumed by fire assuming a unit emission factor (1 kg kg^{-1}), thus allowing for a direct comparison to the source FBP calculations. Afterwards, a multi-model comparison using carbon emissions factors (500 g kg^{-1}) was conducted between GFFEPS and four other published wildfire emissions models and Inventories. Results in both sections were broken down into the 14 regions following Giglio et al. (2006). See Table 2 for the region descriptions and the abbreviations used.

510 5.1 GFFEPS Total Smoke Emissions

Figure 9 shows the regional, annual values of (a) smoke emissions, (b) burned area and (c) average total fuel consumption per unit area. Total smoke emissions and burned area are directly estimated by the GFFEPS model. Average total fuel consumption per unit area was calculated as smoke emissions over burned area for the analysis regions. The annual emission totals allowing a comparison of regional model results to the original FBP fuel consumption calculations.
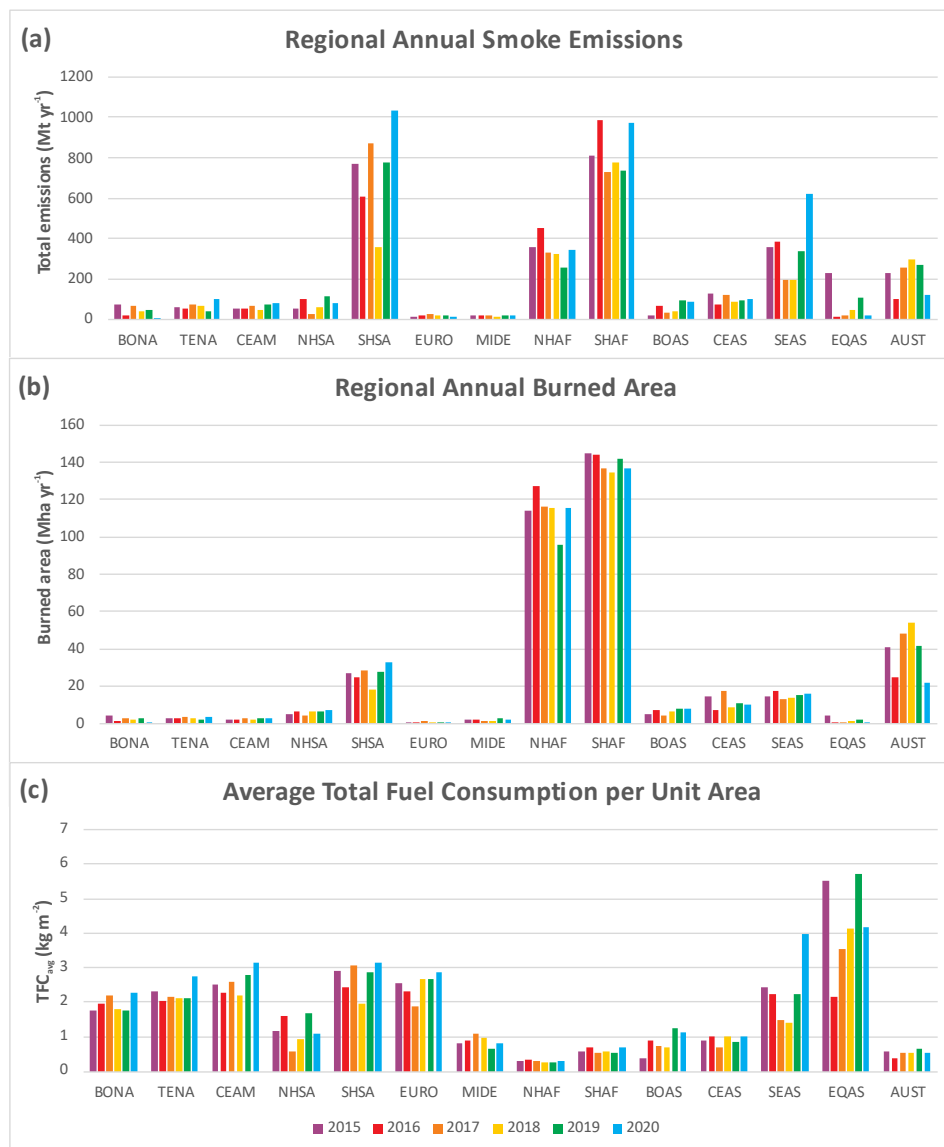
515

Figure 9. (a) Regional annual total emissions (Mt yr⁻¹), (b) regional annual area burned (Mha yr⁻¹) and (c) average total fuel consumption per unit area (kg m⁻²) as predicted by GFFEPS for 2015-2020. Total emissions reflect all smoke emissions released from fires with unit emission factor, equaling to the total fire fuel consumption. See Table 3 for descriptions of regional abbreviations.

520   Total smoke emissions over the six consecutive years, as shown in Fig. 9(a), indicate the largest emitters being SHAF and SHSA, with average annual smoke emissions of 834 and 736 Mt, respectively. Interannual values are relatively consistent through most regions, with the largest range (maximum/minimum) occurring in EQAS (225/12 Mt), BONA (71/6 Mt), BOAS (94/18 Mt) and NHSA (109/24 Mt). El Niño likely drives the variability in EQAS, while fire weather conditions likely determine the variability in the two boreal regions. The figure also shows possible impacts of El Niño and changing

525   deforestation legislation in Brazil, affecting South American emissions (El Niño years are 2016, 2018 and 2019).

Figure 9(b) shows the burned area per region per year. Sub-Saharan Africa (NHAF+SHAF, but excluding MIDE) dominates the global burned area at 254 Mha (69%) of the global average 368 Mha burned annually. This is followed by 38.5 Mha in AUST and 32 Mha in South America (NHSA+SHSA).

The regional burned area predicted by GFFEPS can be compared to national statistics reported by certain countries.

530   Model results indicate that on average 2.06 Mha yr^{-1} in BONA (Canada and Alaska) during the 6 study years. For the same period, Canada's National Forest Database reported 2.19 Mha (http://nfdp.ccfm.org/en/data/fires.php, last accessed 2023-11-10) while Alaska Department of Natural Resources reported 0.64 Mha (https://forestry.alaska.gov/firestats/index, last accessed 2023-11-10). The sum of the two reported values being 2.83 Mha yr^{-1}, which exceeds the GFFEPS prediction by 0.77 Mha. Similarly, GFFEPS predicted on average 2.77 Mha yr^{-1} in TENA, while US agencies reported 3.18 Mha yr^{-1} in the lower 48

535   states for the same six years (https://www.nifc.gov/fire-information/nfn, last accessed 2023-12-15). While GFFEPS estimates only 73% and 87% of the observed values respectively, a correlation between modelled and reported annual values for the six years is strong in each region (r^2 = 0.968 in BONA; r^2 = 0.914 in TENA, not shown). This suggests the methodology for estimating burned area is appropriate. Finally, the quality of fire mapping by agencies, such as whether unburned areas within fire perimeters are properly mapped, may impact these findings, as well as limitation in the MODIS estimates of burned area,

540   but this is beyond the scope of this study.

Average total fuel consumption per unit area by year and region, as shown in Fig. 9(c), was calculated as smoke emissions over burned area from the annual results. Globally, the average is 0.81 kg m^{-2}, while regional results vary from 0.30 kg m^{-2} in NHAF to 4.21 kg m^{-2} in EQAS. Figure 9(c) clearly show regions dominated by forest (e.g., BONA, TENA and CEAM) as having higher fuel consumption per unit area on a global basis compared to those dominated by grasslands (e.g.,

545   NHAF and SHAF). The figure also shows regions strongly affected by El Niño events (EQAS) with annual consumption rates doubling in El Niño years (2015, 2019).

Figure 10 shows the regional daily smoke emissions for the six study years by day of year. Largest emissions occur in SHAF during the region's dry season (mid-May to mid-September) and in SHSA at the end of the dry season (August to mid-October). The latter would be consistent with deforestation burning (Pereira et al., 2022).
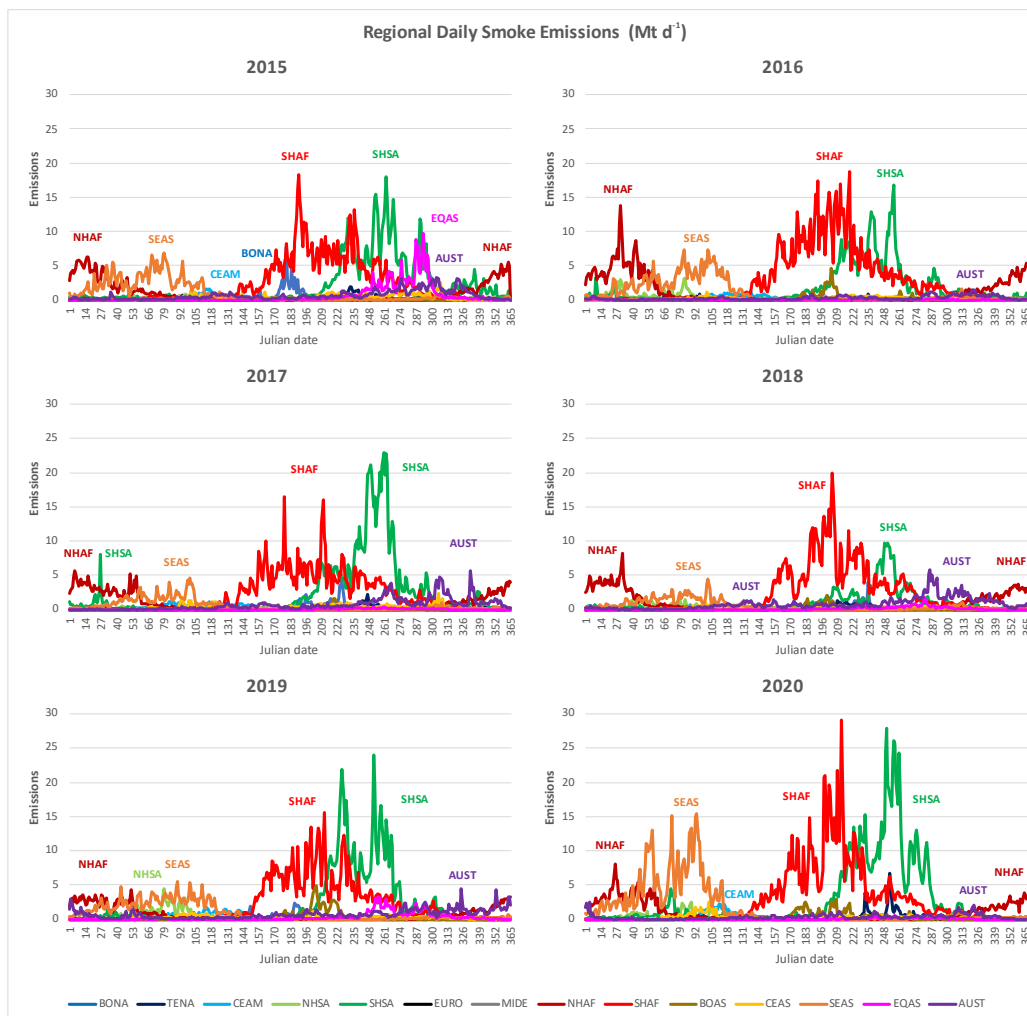
550

Figure 10. Regional daily emissions (Mt d⁻¹) for GFFEPS for the six study years as predicted by GFFEPS. Total emissions reflect all smoke emissions released from fires, equal to the total fuel consumed by fire (carbon emissions would be approximately 50% of the total emissions). See Table 3 for descriptions of regional abbreviations.

555 **5.2 Comparison of GFFEPS to other Wildfire Emissions Models and Inventories**

As noted above, the GFFEPS model was run for six consecutive years (2015 to 2020). Results for global carbon emissions were compared to published results for

- GFAS (Kaiser and van der Werf, 2022, https://www.ecmwf.int/en/forecasts/dataset/global-fire-assimilation-system , last accessed 2024-01-24)
560
- GFED4.1s (van der Werf et al., 2017, https://www.geo.vu.nl/~gwerf/GFED/GFED4/, last accessed 2023-08-11),
- FINN version 1.5 (Wiedinmyer et al., 2011, https://www.acom.ucar.edu/Data/fire/, last accessed 2023-08-11),
- FINN version 2.5 (Wiedinmyer et al., 2023, https://rda.ucar.edu/datasets/ds312.9/dataaccess/, last accessed 2023-08-11).

Annual values of global carbon emissions for all five models are presented in Fig. 11. Results show a wide range of
565   values from 1166 Tg C yr^{-1} in 2018 by GFFEPS to 4231 Tg C yr^{-1} in 2019 For FINN 2.5. In half of the years, GFFEPS produced the lowest results with values ranging from 1166 to 1789 Tg C yr^{-1}. Compared to the other models, GFFEPS estimated values lower than GFAS/GFED (80%/74%), while it estimated values similar to FINN1.5 (97%). The lower values are largely attributed to the inclusion of daily fire behaviour in the combustion completeness calculations, not accounted for in the other models.
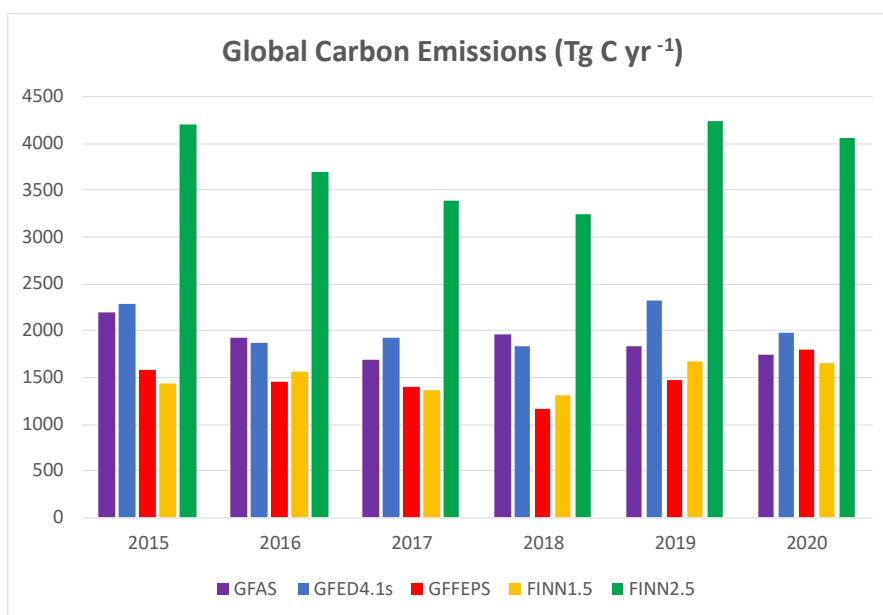
570

Figure 11. Annual carbon emissions (Tg C yr^{-1}) of GFFEPS and other global wildfire emissions models included in this study.

Figure 12 shows a comparison of average annual regional carbon emissions from GFED4.1s and GFFEPS (regional
575   values were not readily available for the other models). The regions of largest GFED emissions are much lower in GFFEPS.

Sub-Saharan Africa (NHAF+SHAF) accounting for 1007 Tg C (49.5% of the total global emissions) in GFED, is reduced to 588 Tg C (39.8%) in GFFEPS. On the other hand, South America (NHSA+SHSA) increases from 304 Tg C (14.9%) in GFED to 403 Tg C (27.2%) in GFFEPS. Also, GFFEPS has greater emissions in six of the 14 regions: CEAM, SHSA, EURO, MIDE, CEAS and SEAS. These are areas dominated by agricultural burning, highlighting the impact of using FAO's crop-burning statistics.
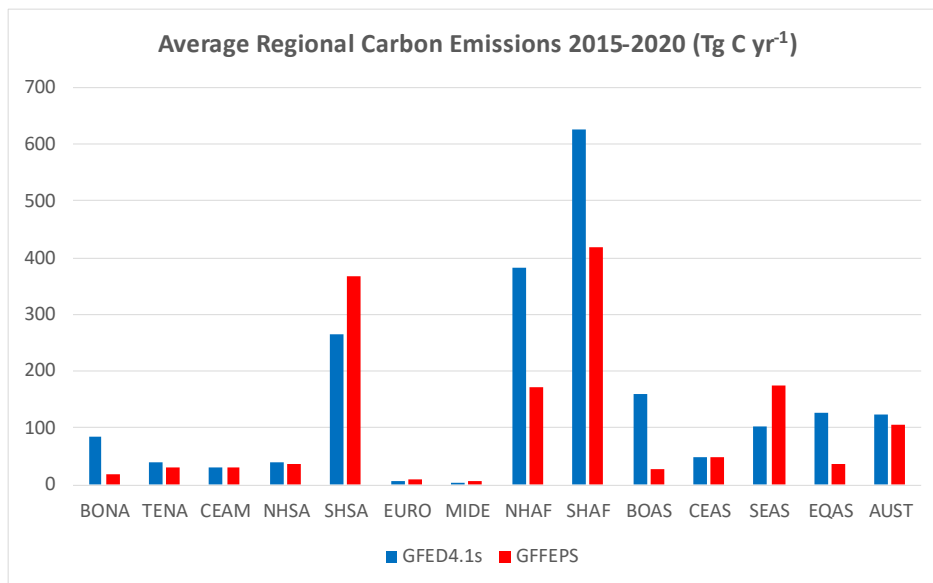
Figure 12. Average annual emissions (Tg C yr^{-1}) by region for GFED4.1s and GFFEPS. See Table 3 for descriptions of regional abbreviations.

Figure 13 shows the annual burned area from the MODIS burned area (MCD64A1) that is used by GFED prior to incorporating small fires, GFFEPS and FINN 1.5/2.5. GFFEPS is in line with most area-burned statistics including the MODIS burned area (MCD64) and FINN 1.5, while FINN 2.5 appears to estimate twice the burned area of the other models.
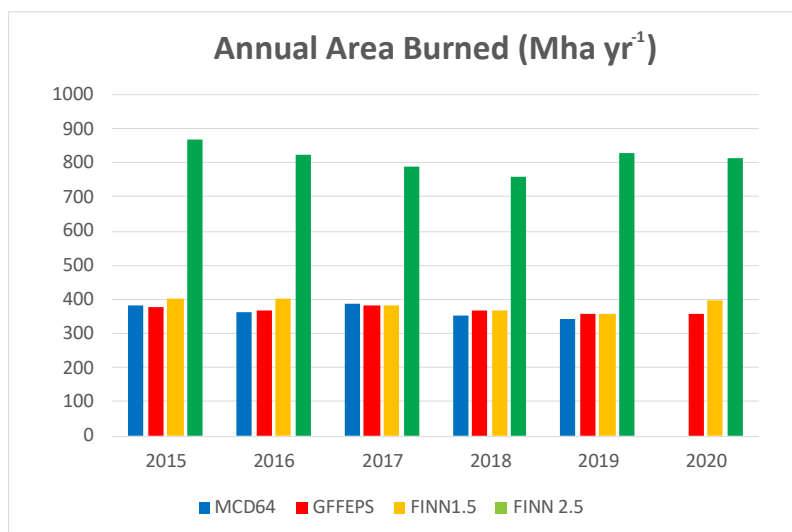
Figure 13. Annual area burned (Mha yr⁻¹) of GFFEPS and other global wildfire emissions models included in this study. The MCD64 data reflects the area burned data used by GFED (prior to small fire adjustments).

Daily burned-area values are available in FINN products allowing a comparison between GFFEPS and the two FINN implementations. Figure 14 shows a sample comparison (2017) between GFFEPS and FINN 1.5/2.5. This pattern is similar to other years. A comparison of daily area-burned values suggests a pattern of results where GFFEPS burned area consistent with FINN 1.5 (MODIS-based). Simple regressions indicate correlations (not shown) of r^2=0.61 between GFFEPS and FINN 1.5 and 0.71 between GFFEPS and FINN 2.5 (when the intercept is forced to zero, the correlations increase to 0.92 and 0.94 respectively). The close agreement between GFFEPS and FINN 1.5 reflects their mutual dependence on MODIS data for burned area; FINN 2.5 follows an alternate methodology of calculating burned area based on aggregating daily observed hotspots into defined fire perimeters. This approach increases the burned area by a factor of two, which is reflected in the higher carbon emissions shown in Fig. 11. GFFEPS shows lower area-burned amounts during Feb-Mar and higher during Oct-Nov. This may be occurring during harvest periods when small fires dominate some landscapes.
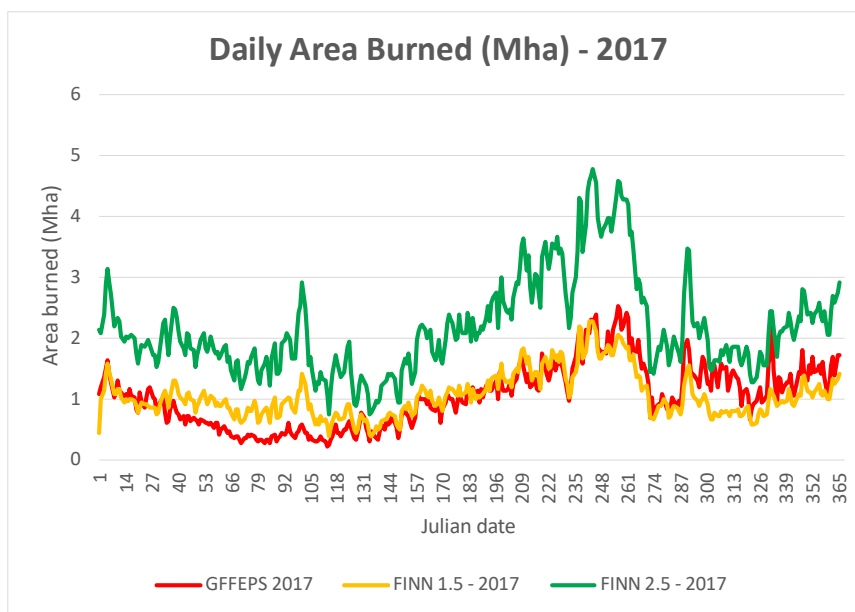
Figure 14. Daily area burned globally (Mha d⁻¹) for GFFEPS and FINN1.5/2.5 for the study year 2017.

6 Discussion

There are no direct measurements of global fire emissions and thus there is no definitive answer as to which of the five
models/versions examined in this study provides the best estimate of fire emissions on a global scale. Based on the principles
of fire, physics and remote sensing, we demonstrated that the GFFEPS general approach to global fire emission estimates are
reasonable and realistic. Pan et al. (2020) demonstrates the range of predictions from six models, while this manuscript shows
the range of predictions among three published models and GFFEPS.

Results from six consecutive years of emissions comparisons show that the GFFEPS model is in general agreement
with well-established models. With regards to the similarities between GFFEPS and GFED4.1s, this should not be a surprise
as much of the GFFEPS methodology and input data is similar to that used in GFED4.1s. Nonetheless, the key essential
difference between the two models is that GFED4.1s uses static fuel loads and consumption completeness, while GFFEPS
models these dynamically, both spatially and temporally, achieved by using the well-established CFFDRS with FBP fuel
consumption driven by FWI fire weather. While the underlying CFFEPS system was designed for Canada and North America,

620   model results show that the approach making use of CFFDRS parameters is robust and adaptable to conditions beyond North America.

The benefit of producing the three components of Fig. 9 is important as that it helps to validate the GFFEPS calculations. While we cannot directly measure global emissions, we can measure certain components. The burned area (Fig. 9(b)) can be directly compared to national statistics where available, while the total fuel consumption per unit area (Fig. 9(c)) appear to fit

625   within expected values for various landscapes. Together, they indicate the calculated global emissions (Fig. 9(a)) produced by GFFEPS are realistic. Further refinement of the burned area and fuel consumption models will then help to improve model accuracy.

Figure 9 also helps to illustrate the source of variability in global emissions. For example, the figure shows the magnitude of smoke emissions (Fig. 9(a)) in sub-Saharan Africa is primarily a result of the burned area (Fig. 9(b)) by low-

630   intensity fires, as indicated by the low value for the total fuel consumption per unit area (Fig. 9(c)). Conversely, higher fuel consumptions (Fig. 9(c)) are shown in the forested regions in North America while variable consumptions in southeast and equatorial Asia reflect the impact of El Niño on the regions.

When compared to other models, differences in estimated carbon emissions appear between the models within and across regions. Indeed, each of the models may be superior at modelling emissions in specific regions, while weaker in others.

635   Evaluating regional variability is beyond the scope of this study. Other factors appear in the inter-annual results such as possible impacts of changing deforestation burning policies in Brazil as emissions vary from year to year (Fig. 9(a); Schmidt and Eloy, 2020). El Niño events have been linked to global fire activity and emissions, and representation of this in weather data used by models can vary and appear linked to emission differences as impacts to southeast and equatorial Asia in 2015 and 2019.

640   The GFFEPS model is largely based on the well-established CFFDRS system of fire behaviour and fuel consumption and the regional CFFEPS fire emissions model. The inclusion of the CFFDRS system allows for a clear and scientific method to directly incorporate NWP model forecasted meteorological conditions, near-real-time fire location measurements, and fuel moisture estimates as driving forces in daily fire activity accounting and emission calculations. Of the models presented in this study, GFAS and FINN provide comparable, near-real-time products; while these models include forecasted weather and

645   fire locations, they do not address the near-real-time dynamic fuel moisture and fire behaviour captured by the CFFDRS as used in GFFEPS.

Extending the CFFDRS to a global environment was a challenge, and in this initial global application exercise, several important assumptions were made. One such assumption was the introduction of the *GSI* as a means for modelling plant phenology responses in predicting seasonal leaf-out of deciduous forests, and grass curing though a *DC*-based approach.

650   Applying these effects on fuel consumption was understandably unaddressed in the original, Canadian-focused, FBP system. Canada's fire danger group focused much of its attention on hazardous fuels, capturing spread rates and fire behaviour in the situations that threaten fire fighter and community safety; little attention was made for the aftermath of fire activity in terms

of accounting for smoke and carbon emissions in the 1970s through 1990s when the Canadian FBP system was developed. Also, green grass and leaf-out deciduous posed little threat and thus received cursory assumptions.

655   Another issue in extending CFFEPS to a global domain was the lack of data from field experiments and measurements outside of Canada encompassing more diverse environment conditions. This was required not only for validation, but also for building a parameterization to expand the FBP approach to modelling fire behaviour in a broader domain. Papers such as Hoffa et al. (1999) and Shea et al. (1996) were invaluable in understanding fires in African savannah. There again, the authors focused their attention on the dry season and highest flammability, and this may influence GFFEPS results outside of these

660   high-burning seasons.

The methodology of assigning burned area per hotspot with the burned-area climatology dataset was an early assumption of CFFEPS carried over into GFFEPS. It provides a means of deriving burned area for near-real-time, model forecast operational applications as compared to the hindcast, retrospective approach used in most other global fire emissions models. Discrepancies did arise, as evident in current 2016-2020 comparison where GFFEPS underestimates burned area in

665   boreal and temperate North America relative to nationally-reported statistics.

Incorporating small fires was recognized as a non-negligible issue. Researchers developing the GFED model focused efforts into extrapolating burned area by small fires from coarser-resolution data, whereas, the use of FAO crop-burning statistics in GFFEPS provided an alternate route. While small fires may have some impact on fires outside of the agricultural zone, it was deemed an acceptable route given the relative contribution of agricultural fires compared to wildfire emissions.

670   GFFEPS follows the satellite-based fire detection methodology and is faced with the traditional issues associated with that approach, namely restricted by satellite-overpass times, sensor resolution, observational swath width, heavy smoke and cloud cover. Other limitations of the bottom-up approach used by GFFEPS include land-cover and burned-area mapping resolution as well as the accuracy of fuel load mapping and fuel consumption modelling.

The GFFEPS model as presented in this manuscript is intended as a proof of concept: we have demonstrated the ability

675   to model fuel consumption dynamically and its utility for forest fire emissions simulations, particularly in near-real-time forecasting applications, on a global level. There is still much work to be done. Many of the spatial components, specifically FBP fuels and fuel load assignments, need more rigorous examination and validation. A number of assumptions and generalizations were made to allow the model to function using global input data. Further work is required to improve on and validate these initial findings. The model as developed is adaptable and open to improvements.

680   Efforts are currently underway to validate GFFEPS against TROPOMI measurements, similar to Canada-only plume rise (Griffin et al., 2020) and CO emissions (Griffin et al., 2023) exercises that have yielded favourable results. Other regional studies may provide additional validation data through remote sensing, particularly on a regional or individual fire basis. For example, Nguyen and Wooster (2020) estimated biomass burning in Africa using geostationary fire radiative power (FRP) and aerosol optical depth (AOD); Hayden et al. (2022) conducted airborne measurements of 193 compounds from 15 instruments,

685   including 173 non-methane organics compounds (NMOG) downwind of a small peat-dominated wildfire at La Loche, Saskatchewan, as part of the Alberta oil sands field study; Adams et al. (2019) used remote sensing to directly measure CO,

NH$_3$ and NO$_2$ from the 2016 Horse River fire near Fort McMurray, Canada, while Stockwell et al. (2022) conducted similar measurements over western US fires. Applying such approaches on a global scale would be beneficial to validating GFFEPS as well as assessing the feasibility in further applications with global chemical transport models.

690   Future direction of the GFFEPS model includes integration with the GEM-MACH chemical transport model, and running the model operationally to provide boundary data and input for the regional CFFEPS model. This would allow for the transcontinental transport of smoke emissions into the air-quality forecasts for Canada. Efforts are underway to link CFFEPS with a predictive fire-growth model (Anderson et al., 2009) and coupling the impact of smoke plumes generated by CFFEPS on ground temperatures as presented in public forecasts (Makar et al., 2020). Finally, initial steps have begun to link

695   GFFEPS to the Canadian Earth System Model (CanESM5; Swart et al., 2019) and the Canadian fourth generation atmospheric global climate model (CanAM4; von Salzen et al., 2019) for integrated study of climate driven impacts on regional wildfire risks, and air quality analysis.

7 Conclusion

    This paper presents the Global Forest Fire Emissions Prediction System (GFFEPS) as a model to estimate emissions of

700   smoke from biomass burning globally. Based on the regional Canadian Forest Fire Emissions Prediction System (CFFEPS), the methodology has been extended to a global environment. Both systems are based on the well-established Canadian Forest Fire Danger Rating System. By using forecasted 3-hour meteorological conditions produced by Environment and Climate Change Canada's Canadian Global Elemental Multiscale (GEM) model, daily fire weather calculated with FWI, and fire behaviour, fuel consumption estimated from FBP, the GFFEPS model is shown to produce estimates fire emissions in an

705   operational setting.

    The model uses a bottom-up approach and is based on remotely-sensed hotspot locations and predicted burned area. Using forecasted meteorological conditions, daily fire weather, and a global land classification at a 1-km resolution, GFFEPS provides dynamic estimates of fuel consumptions in near-real time, differentiating it from other global emissions models. A study was conducted running GFFEPS through a six-year period (2015-2020). Results were compared to other global

710   emissions models including GFAS, GFED4.1s and FINN1.5/2.5. GFFEPS estimated values lower than GFAS/GFED (80%/74%), while it estimated values similar to FINN1.5 (97%). Differences are largely due to its inclusion of daily weather as predicted by the GEM model and fire behaviour modelling provided through the CFFDRS.

    This manuscript presents the initial release of the GFFEPS model. Its development is on-going and future avenues are recognized and being pursued, including incorporating the model to existing air-quality models, coupling CFFEPS/GFFEPS

715   with predictive fire-growth models, and linking the model to global climate models. This paper presents the methodology currently used in the model, and shows it providing realistic results in line with other models. Efforts are underway to validate the model, improve its sub-components and expand its use to other global air-quality and climate models.

8 Appendix A. Supplemental Information: Fuel Consumption Models

720   Efforts to validate fuel consumption models used in GFFEPS were conducted using data from published studies. These studies documented observed weather, fire behaviour and fuel consumption associated with prescribed fires in specific landscapes and forest stands. These results are compared with fuel consumption predicted by GFFEPS and by GFED4. GFFEPS follows the Canadian Forest Fire Danger Rating System (CFFDRS, Stocks et al., 1989), specifically, the Canadian Forest Fire Weather Index (FWI) system (Van Wagner 1987) and the Canadian Forest Fire Behavior Prediction (FBP) system

725 (Forestry Canada Fire Danger Group 1992; Wotton et al., 2009). To calculate fuel consumption, GFFEPS requires:

- a fuel model compatible with the FBP system,
- FWI values on the date of the fire,
- latitude, longitude, and Julian date for Foliar Moisture Content (*FMC*) calculation,
- daylength and vapour pressure deficit for Growing Season Index (*GSI*) calculation (Jolly et al., 2005).

730   GFFEPS uses the Global Land Cover 2000 Project (GLC2000, Bartholome and Belward, 2005) to determine fuel models. GLC2000 provides spatial land cover classifications for the globe at a 1-km resolution. For the purposes of validating fuel consumption, a representative GLC2000 classification, shown in italics (e.g., *needle-leaved, evergreen*), was selected for each study landscape.

     Historical fire weather values were taken from a high-resolution (0.25°) global re-analysis of fire weather conditions
735 from 1979 to 2018 (McElhinny et al. 2020), except when values were included in specific studies (Alexander et al., 1991, Stocks et al., 2004, Stocks 1989, Stocks 1987a, Stocks 1987b, Quintilio et al., 1991). Duff moisture Codes (*DMC*) and Drought Codes (*DC*) were retrieved and from these, Buildup Indexes (*BUI*) were calculated following the FWI system equations. For the purposes of this study, daily values of *GSI* were used in place of 21-day averages as historical weather to calculate a 21-day average were not readily available (historic papers typically included meteorological values the day of observed burns
740 alone).

     Given the input represented or derived from observed data in each individual study, predicted GFFEPS fuel consumption was calculated using the FBP system equations. Fuel loads, largely based on van Leeuwen et at. (2014), were used as global default values in the FBP calculations (see 4.2 Fuel Load); regional fuel load values presented in this supplemental information section replace global defaults. Consumption rates following the GFED methodology are also
745 presented for comparison. Note that GFED values are based on version 4.1s fixed fuel loads and consumption rates per region and fuel with no allowance for variable meteorology and fire weather (see 1.0 Introduction).

A.1 Boreal Forest

     The Canadian Forest Fire Behaviour Prediction (FBP) System is based on case studies of fire behaviour in the Boreal Forest (Table A.1). These studies include fuel loads and depths, noon weather observations (temperature, relative humidity,

750   wind speed, etc.) as well as the calculated FWI values (*FFMC*, *DMC*, etc.). Fuel loads used in GFFEPS were based on default

values in the FBP manual.

Table A.2. Canadian Forest Fire Behavior Predictions (FBP) System fuel types included in this study.

FBP	Fuel description	Reference	Surface fuel load (kg/m^2)	Crown fuel load (kg/m^2)
C-1	Spruce–Lichen Woodland	Alexander *et al.* 1991	1.5	0.75
C-2	Boreal Spruce	Stocks *et al.* 2004	5.0	0.8
C-3	Mature Jack Pine	Stocks 1989	5.0	1.15
C-4	Immature Jack Pine	Stocks 1987a	5.0	1.20
M-3/4	Dead Balsam Fir Mixedwood–Leafless	Stocks 1987b	5.0	0.8
D-1	Leafless Aspen	Quintilio *et al.* 1991	1.5	*

*Crown fuel load for D1 is not applicable

755   **A.1.1 Coniferous**

The GLC2000 lacks the detail required to distinguish all the fuels presented in these studies. Instead, *needle-leaved, evergreen* land cover classification is represented in GFFEPS simply as a C-2 (boreal spruce) fuel type for North America. GFFEPS thus uses the C-2 surface fuel consumption calculation with the default C-2 surface fuel load of 50 t ha^{-1} and an average crown fuel load of 10 t ha^{-1} as documented in the FBP manual.

760   Figure A.1 shows the scatter plot of observed versus predicted total fuel consumption. Predicted values are based on GFFEPS calculations, assuming all fuels as C-2 (boreal spruce) fuel type, while using the observed using weather conditions from the source papers. The resulting correlation coefficient (r^2) was 0.416. Forcing the regression through the origin, we find the predicted data is overpredicting the observed fuel consumption by only 2.5%.
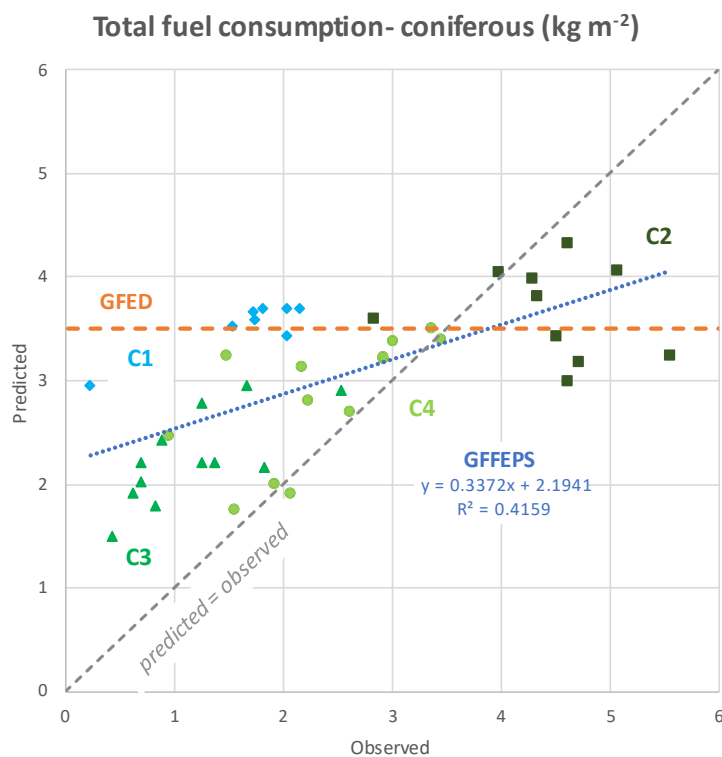
Figure A.1. Observed total fuel consumption vs GFFEPS predictions for Boreal coniferous forests assuming all fuel as C-2. Points coloured to reflect the fuel type from each study. The constant value of GFED predictions (3.5 kg/m²) is shown as an orange dashed line.

765

Using a fuel load of 69 t ha^{-1} with a combustion completeness of 51%, GFED predicts a fixed fuel consumption 3.5 kg m^{-2} for Boreal Forest, regardless of season, and does not distinguish between conifer and deciduous (van Leeuwen et at., 2014).

770

A.1.2 Deciduous

Deciduous stands in the Boreal Forest are represented by aspen in the CFFDRS. Quintillio et al. (1991) documented spring fires in leafless aspen stands in central Alberta. Note that one reported burn was removed from this comparison. As the authors wrote:

775   "Two of the plots were jointly reburned, and, among other data, a 10-fold increase in fire intensity was documented, due largely to aspen mortality in 1972 and the subsequent increase in fuel load."

These two reburned plots (their 3b&c) were reported as a single data point with fuel consumption of 3.402 kg m^{-2}, which exceeded the default fuel load of 15 t ha^{-1} (1.5 kg m^{-2}). The frontal fire intensity of this fire was 57,261 kW/m. Including this point would skew the regressions and thus were removed.

780   Using the original study results (less the removed plots), observed fuel consumptions were compared to those predicted by GFFEPS. The default FBP surface fuel load of 15 t ha^{-1} was used in the GFFEPS calculations. The Growing Season Index (*GSI*) was then introduced as a modifier to the predicted fuel consumption, with *GSI* values ranging from 0.0 to 0.55 with an average of 0.18 (see Eq. (9) under 4.3 Combustion Completeness).

Figure A.2. shows the scatter plot of observed fuel consumption versus that predicted by GFFEPS. Including *GSI* in the

785   calculations changed the regression from a negative correlation ($r^2 = 0.037$) to positive ($r^2 = 0.221$).

There is no clear fuel type in GFED that represents North American aspen forests (van Leeuwen et at., 2014). They report a fuel consumption of 3.5 kg m^{-2} for the Boreal Forest, and 5.8 kg m^{-2} for the temperate forest (fuel load of 115 t ha^{-1} and combustion completeness of 61%), both of these values exceed all observed values in Quintillio et al. (1991).
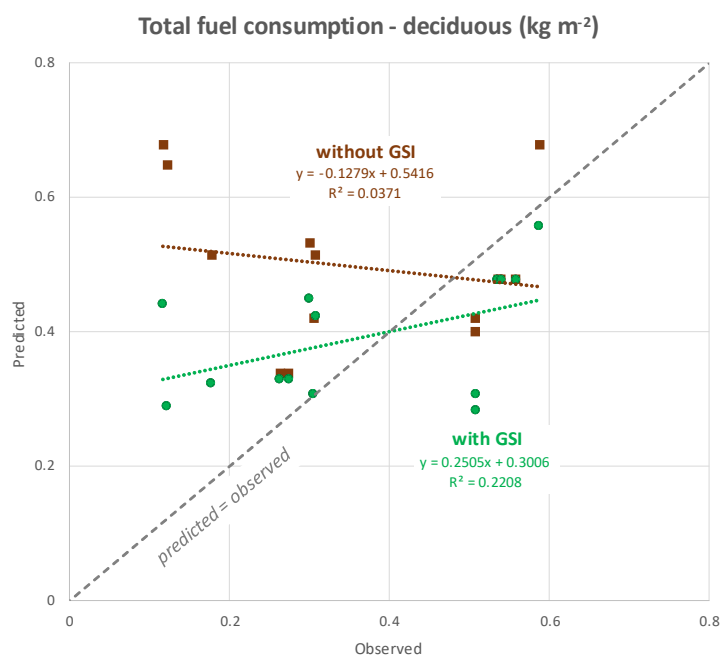
790

Figure A.2. Observed total fuel consumption vs GFFEPS predictions for Boreal deciduous forests. Green and brown indicates the use of GSI as a modifier for greenup in fuel consumption calculations. Dotted lines show regressions through respective datasets.

795

Note that as the only deciduous fuel type in the FBP system, D-1/2 (leafless/ leafed) aspen fuel type was used globally to represent a number of *broadleaved* land cover types in GLC2000 used by GFFEPS. Fuel loads and greenness varied between regions and classifications.

A.1.3 Siberia

800 McRae et al. (2006) studied fire behaviour in Scotch Pine forests in central Siberia. Following the same methodology as Canadian forests, study results were compared to predictions based on GFFEPS. Foliar moisture content (*FMC*) equations developed for Eurasia were used as described in the manuscript.

The reported results were compared to each of the seven FBP coniferous fuel types as well as the M-3/4 - Dead Balsam Fir mixedwood fuel type. Table A.2 summarizes the regression results. Immature jack pine (C-4) provided the best fit to the

805 data ($r^2 = 0.921$) while mature jack pine (C-3) provided the fit closest to unity ($a = 1.036$) and C-2 was closest to intercepting the origin ($b = 0.165$). Figure A.3 shows scatter plots of the study data against GFFEPS predictions using fuel types with the best results.

Table A.2. Summary of correlation coefficients (r^2) of study-based observed fuel consumptions in Scotch

810 **pine versus GFFEPS predictions using various FBP fuel types. Best fits per column are shown in bold.**

	Surface fuel load (kg/m²)	Crown fuel load (kg/m²)	r^2	a (slope)	b (intercept)
C-1	1.5	0.75	0.300	0.351	0.51
C-2	5	0.8	0.852	0.846	**0.165**
C-3	5	1.15	0.873	**1.036**	0.449
C-4	5	1.2	**0.922**	1.28	-0.763
C5	5	1.2	0.894	0.731	-0.337
C6	5	1.8	0.894	0.731	-0.337
C7	1.75*	0.5	0.620	0.469	1.638
M-3/4	5	0.8	0.805	0.704	0.787

*Surface fuel load of C7 is a blend of forest floor (2.0 kg m⁻²) and woody fuel loads (1.5 kg m⁻²).
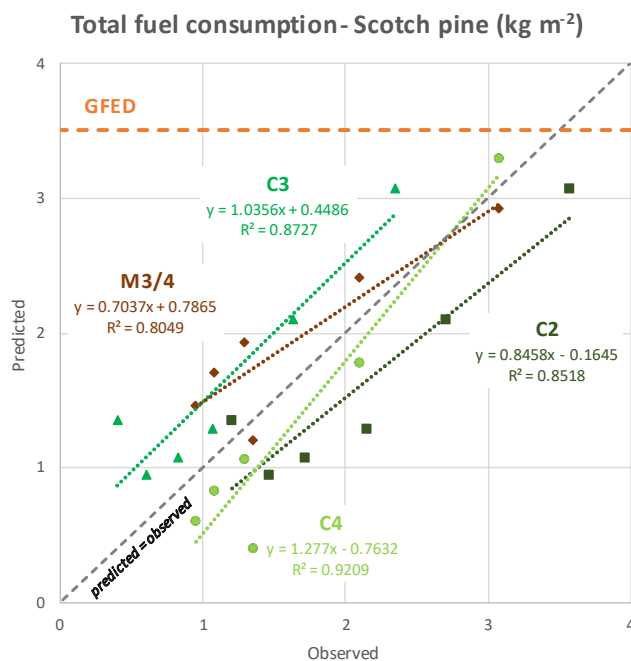
Figure A.3. Observed total fuel consumption for central Siberian Scotch pine forest vs GFFEPS predictions using various FBP fuel types. Dotted lines indicate regression lines for respective fuel types. The constant value of GFED predictions (3.5 kg/m^2) is shown as an orange dashed line.

It is expected that Scotch pine forests are best represented by the FBP mature and immature pine fuels found in Canada. With that said, Siberia, like Canada, is covered by a wide variety of coniferous and deciduous forests. A large component of these are larch forests that lose their needles every winter. No studies were found for comparative purposes.

For GFFEPS purposes, a C-2 – boreal spruce fuel type was used for *tree cover, needle-leaved, evergreen* in northern Eurasia, northeastern Europe and North America; C-3 – mature jack pine in remaining areas. Fuel loads varied between regions.

A.2 Tropical Forest

A validation of model calculations against original source material was conducted for tropical fires in the Amazon. Source materials used were readily available papers referenced by van Leeuwen et al., 2014 (Carvalho et al., 1995; Fearnside et al., 1993; Fearnside et al., 2001; Guild et al., 1998; Kauffman et al., 1993; Kauffman et al., 1998; Ward et al., 1992). Fires in these studies were all land clearing, conducted for agricultural use. Trees were typically felled at the onset of the May-September dry season and burned at the end of the dry season. Natural fires in uncleared lands in the Amazon are rare (but

830 are now increasing) and when they occur, they burn in the understorey, likely undetected by remote sensing (Withey et al., 2018).

The most representative classification of tropical rainforest in the GLC2000 land classification categories is *Tree cover, broadleaved evergreen.* Sampling the fire locations on the GLC2000 spatial dataset:

- 8 fires occurred in *Tree Cover, broadleaved, evergreen* (Carvalho et al., 1995; Fearnside et al., 1993; Fearnside et
835 al., 2001; Guild et al., 1998; Kauffman et al., 1998)

- 2 fires occurred near *Tree Cover, broadleaved, evergreen* (Kauffman et al., 1993; Ward et al., 1992),

- 3 fires occurred in *Bare Areas*, but described in the text as 12-year regrowth after slash-and-burn (Kauffman et al., 1993),

- 4 southern fires in *Herbaceous Cover, closed-open* were described as savanna and left out of analysis (Ward et al.,
840 1992),

where near is defined as having an adjacent cell categorized as *Tree Cover, broadleaved, evergreen* on the 1km resolution dataset.

The D-1 - Leafless Aspen FBP fuel type was used for downed trees (hence, greenup was deemed unnecessary). Various slash fuels in the FBP system were also examined but did not improve on the following results.

845 Figure A.4 shows the scatter plot of observed total fuel consumption versus that predicted by GFFEPS. Points have been colour coded based on their general land classification. Including all data points produces a poor correlation ($r^2 = 0.04$) but by removing the outliers associated with burns after recent regrowth and those classified as near, but not within, broadleaf evergreen, increase the correlation to $r^2 = 0.732$.
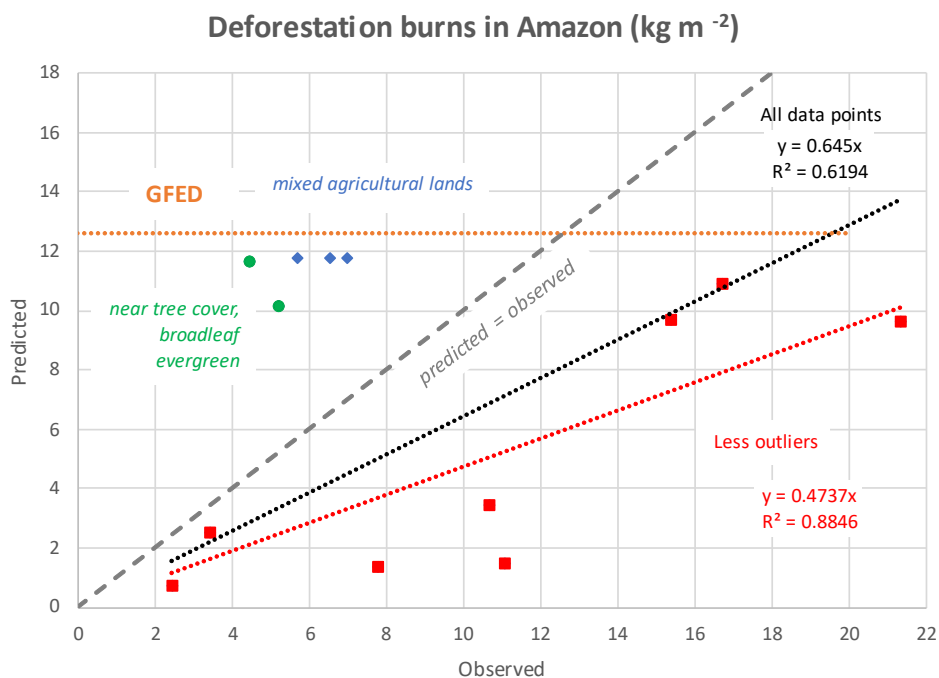
Figure A.4. Observed total fuel consumption vs GFFEPS predictions for tropical forests assuming all fuel as D-1. Points coloured to reflect the general land classification from each study. The constant value of GFED predictions (12.6 kg/m²) is shown as an orange dashed line.

For tropical forests, GFED uses a fuel load of 285 t ha^{-1} and a combustion completeness of 49%, yielding a constant fuel consumption of 12.6 kg m^{-2}. Fuel loads for GFFEPS were calculated following data collected by van Leeuwen et al. but heavier fuels (20.5 cm diameter) were left out (assumed to be uncombusted) to give a fuel load of 117.9 t ha^{-1}. Adjusting this value by a bias correction of 155%, the fuel load becomes to 182.8 t ha^{-1}. The bias correction was based on a decision to include all points. This was made to avoid extreme overpredictions in the fringe areas, in this case representing 5 of the 13 points. All points covered site characteristics inconsistent over the eight published reports and while some studies produced outliers, their overall results were deemed valuable.

The Buildup Index (*BUI*) of the FWI system was compared directly to percent fuel consumed as shown in Fig. A.5. This supports the weather-based approach used by GFFEPS. Lower consumption (<60%) in *tree cover, broadleaved, evergreen* supports excluding heavier fuels from the analysis.
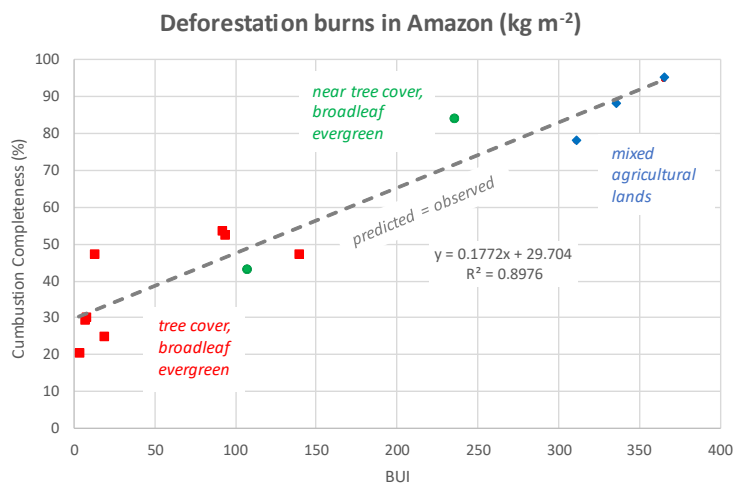
Figure A.5. **Observed Buildup Index (BUI) and combustion completeness at published fire sites. Points coloured to reflect the general land classification from each study.**

A.3 Tropical Peat

Field et al. (2004) studied air quality in western Indonesia using the Drought Code (DC) to predict visibility. In their study, a nonlinear regression model was developed relating visibility and DC. Based on their model, a logistic model for fuel consumption, FC (kg m^{-2}), was built using their point of inflection ($DC = 551$) and shape scale controlling the curvature ($S = 123.7$)

$$FC = 105.6 / (1 + e^{\frac{551-D}{123.7}}) \quad\quad\quad\quad (A.1)$$

where 105.6 kg m^{-2} (1056 t ha^{-1}) is the fuel load from van Leeuwen et al. (2014) for tropical peat.

2015 was an exceptional year for smoke emissions in the region. Kaiser et al. (2016) estimated that over 15% of 2015 global emissions were from fires in tropical Asia. To examine this, hotspots were collected between 0º and 4ºS latitude and 112ºE and 116ºE longitude for 2015. Fuel consumption based on our logistic model was calculated using the daily average DC values of these hotspots (based on the GEM model FWI as described in the manuscript), which ranged from 5.15 to 458.1 and averaged 116.3.

Figure A.6 shows a comparison of daily hotspots and calculated fuel consumption. Both show peak activity in the fall, though the predicted fuel consumption spread is wider than the principal hotspot activity. A background fuel consumption of 1.213 kg m^{-2} results when $DC = 0$. This could be removed in the future but in the absence of hotspots, this may be immaterial.
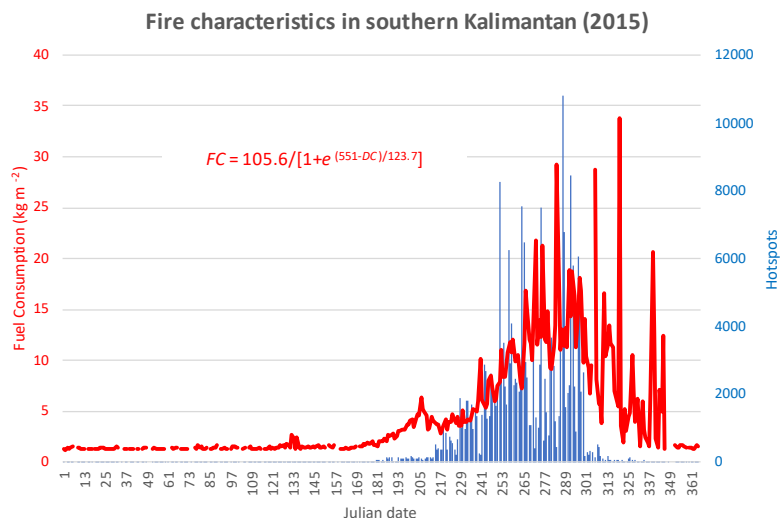
Figure A.6. Fire characteristics in southern Kalimantan for 2015. Hotspot count (blue) represent region between 0º and 4ºS latitude and 112ºE and 116ºE longitude. Fuel consumption (red) based on logistic model and average DC values of hotspots occurring in the region.

Graham et al. (2022) evaluated fire behaviour in drained tropical peatlands, examining smouldering peat fires at five locations in Kalimantan during August and September, 2015. This provided data to validate our logistic model. Fuel consumption was calculated using DCs from the reanalysis data (McElhinny et al. 2020) with all five locations occurring in the same reanalysis grid cell. Choosing representative DC values was an issue as a precipitation event appears to have occurred, as on August 28, 2015 the DC dropped from 443 to 123 in the reanalysis data. This was not noted by Graham et al. and may not have happened at any of the study sites. To test the impact of this event, the adjacent reanalysis cell to the east where the precipitation did not occur was included for comparison. A second alternative was used based on the daily average DC values for hotspots occurring in the study area (between 2.2064 ºS and 2.5226ºS latitude and between 114.39 ºE and 114.63175 ºE longitude) based on an ECCC GEM-MACH model run. These values ranged from 147 to 291, which were higher than average DC of 116.3 for 2015.

Figure A.7 shows a scatter plot of the study data versus GFFEPS predictions. Fuel consumption based on the reanalysis data produced a negative trend, while results based on the reanalysis cell to the east produced consumption values 3 to 5 times higher than those using the average DCs of the hotspot in the area. Linear regressions of the latter two produced correlation coefficients (r^2) of 0.801 and 0.822, suggesting GFFEPS performed well for this tropical peatland location (given its few data points).
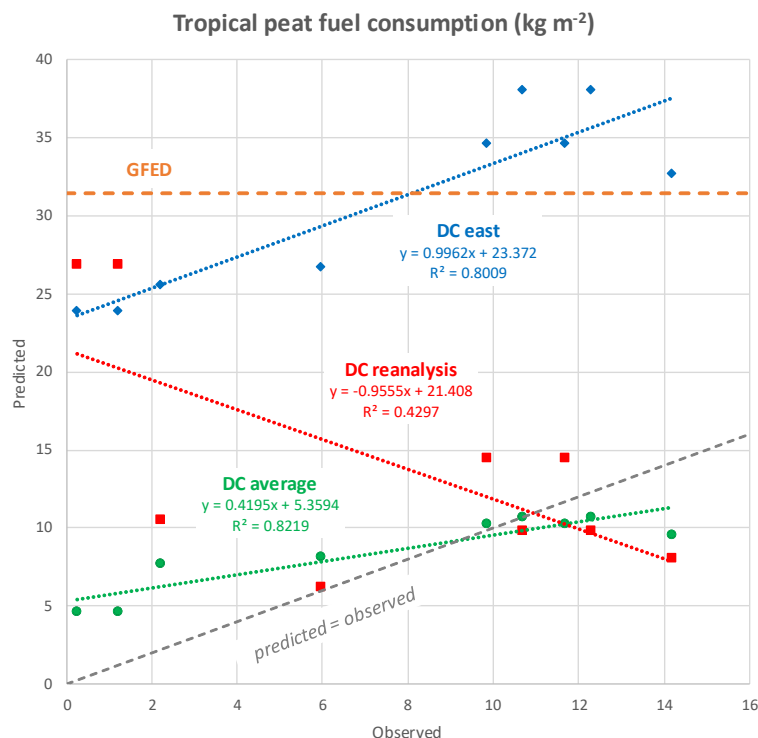
Figure A.7. Observed fuel consumption in tropical peatlands in southern Kalimantan, Indonesia vs GFFEPS predictions. Predicted consumption for the nine data points using the reanalysis DC data (red), DCs using the reanalysis grid cell 27 km due east (blue) and daily DCs averaged from the hotspots occurring in the study area (green). The constant value of GFED predictions (31.4 kg/m²) is shown as an orange dashed line.

For tropical peatland, GFED uses a fuel load of 1056 t ha⁻¹, combustion completeness of 27%, yielding a fuel consumption rate of 31.4 kg m⁻². This value is close to consumption rates observed east of the study.

The observed values were highly variable and this was acknowledged by Graham et al. (2022). The August 28 precipitation event played a significant role, as shown by the data. The *DC* average likely shows the general impact of precipitation on the sites while *DC* east shows the conditions without. In the *DC* reanalysis results, the two outlying points with low observed values (<2 kg m⁻²) and high predicted values (>25 kg m⁻²) may reflect a discontinuity in timing the transition from dry to wet conditions. This is certainly a possibility given these points were from one site sampled on August 20. It is possible that the site received precipitation prior to the August 28 event, yet without on-site weather observations, this is only speculation.

In terms of GFFEPS validation, it appears the predicted values of the *DC* average follow the observed data closely, with a correlation of 0.8219. The dry conditions shown by *DC* east match well with the GFED value but that may be due to the common fuel load value used by both models. Unfortunately, there is no reported precipitation data to be certain as to

920 what happened at the study site. Closer examination of tropical peat fires is in order but such studies are not available in the current literature.

A.4 Wooded and Open Savanna Grasslands

Savanna fires were examined based on original work by Hoffa et al. (1999), Shea et al. (1996) and de Castro and Kauffman (1998) as referenced and used in van Leeuwen et al. (2014). Hoffa et al. (1999) studied 13 prescribed burns

925 conducted in the early dry season (June to August) in Kaoma Local Forest 310, western Zambia (14°52'S, 24°49'E); as part of the South African Fire-Atmosphere Research Initiative (SAFARI) project, Shea et al. (1996) documented 10 fires in Kruger National Park, South Africa (31°14'00"E, 25°15'13"S), three fires in Kasanka National Park , Zambia (12°35'S, 30°21'E) and one near Choma, Zambia (16°50'S, 26°59'E) ; and de Castro and Kauffman 1998 examined fires in the Brazilian Cerrado, a mosaic of savanna and forests near Brasilia, at the *Reserva Ecológica do Instituto Brasileiro de Geografia e Estatística* (IBGE)

930 and the *Jardim Botânico de Brasilia* (JBB) (15°51'S, 47°63'W).

Dambo is an African grassland, seasonally flooded during the rainy season. It occupies 10% of Zambia. Miombo is an open-canopy, semideciduous woodland with a grass and shrub understory. It covers 12% of Africa and 80% of Zambia. In Shea et al. (1996) 12 burns were conducted in dambo grasslands, 2 in miombo woodlands; in Hoffa et al. (1999), 7 burns were conducted in dambo and 6 burns in Miombo. The four Cerrado sites in de Castro and Kauffman (1998) were conducted

935 across a range of densities: *campo limpo* (pure grassland), *campo sujo* (a savanna with a sparse presence of shrubs), and two variants of Cerrado *sensu stricto* (a dominance of trees with scattered shrubs and a grass understorey).

Grass curing, a measure of percent dead/dormant/dry as opposed to live/growing/green grass, is a driving factor in the rate of spread in grass fuels in the FBP system. The system assumes complete consumption of grass fuels – a generalization made by those who developed the system (see 6. Discussion). An alternative approach used by GFFEPS is that grass fuel

940 consumption is related to grass curing following the same relationship as used for rate of spread. Grass typically follows a seasonal pattern of growth during the spring (or rainy season) followed by drying and mortality during the summer (or dry season). Figure A.8 shows the relationship of grass curing (reported as % dormancy) at the burn sites in the three publications and the *DC* from the FWI system as interpreted from the global re-analysis of fire weather conditions (McElhinny et al. 2020). A power law relationship was derived with a correlation of 0.2515. *GSI* was considered as a possible predictor to grass curing

945 but the correlation was negligible in these studies.

2024-03-06
10.5194/gmd-2024-31
Geoscientific Model Development
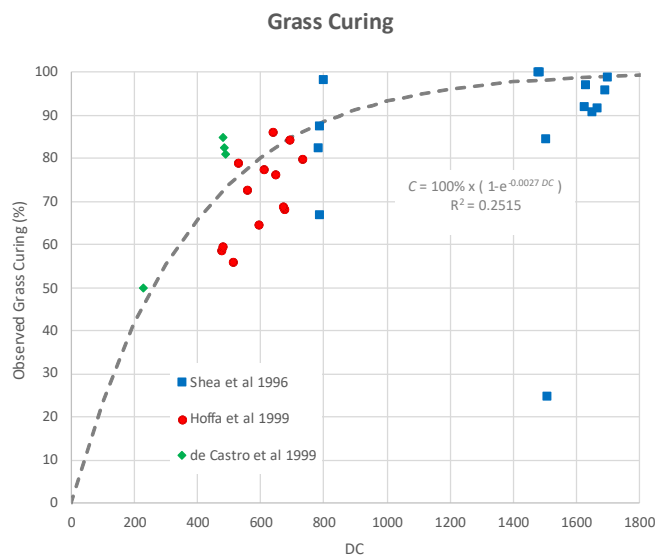
Figure A.8 The relationship of grass curing (% dormancy) to Drought Code (DC) observed at the sites in the three publications.

950  Figure A.9 shows the scatter plot of observed total fuel consumption versus that predicted by GFFEPS. Following GFFEPS methodology, dambo grassland savanna was assigned a standing grass open fuel type (O-1B) with an average total fuel load of 4.0 t ha^{-1} based on the average total biomass reported in Hoffa et al. (1999) and Shea et al. (1996). Fuel consumption was calculated as the product of the grass fuel load and the percent curing. Miombo woody savanna was assigned a leafless aspen fuel type (D-1), given the predominance of down and dead fuels. Fuel load of 9.2 t ha^{-1} was used based on the

955 average total fuel loads. The DCs required for grass curing and BUIs required for D-1 calculations were based on McElhinny *et al.* (2020) global reanalysis (with overwintering). Correlation values (r^2) were 0.312 for dambo grassland and 0.673 for miombo woodland though both were far from the line of equality.
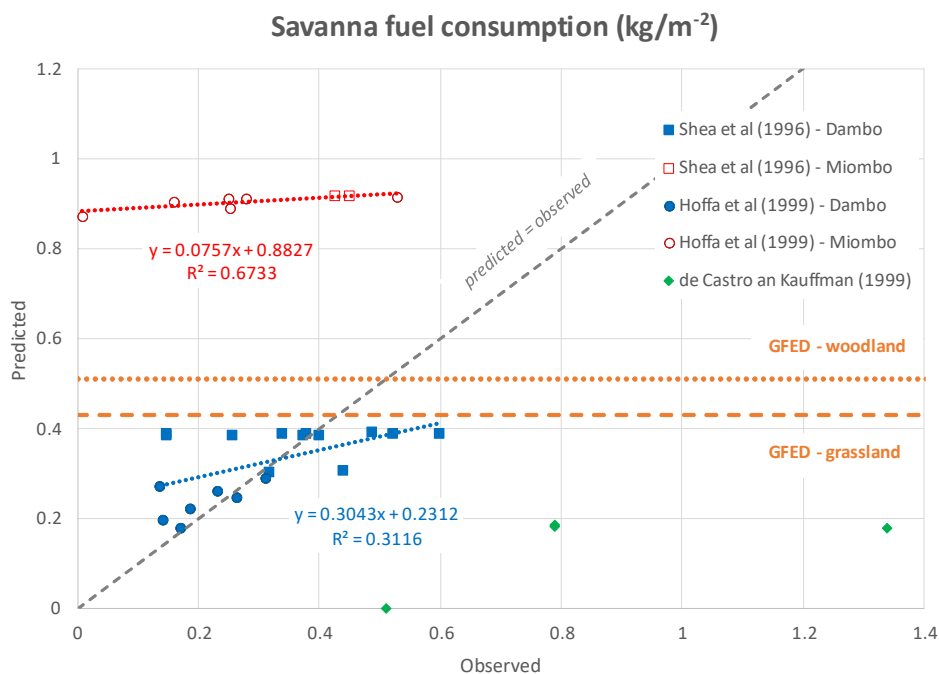
Figure A.9. Observed fuel consumption in dambo grasslands and in miombo woodlands compared to predictions. The constant values of GFED predictions (0.43 and 0.51 kg/m²) are shown as orange dashed and dotted lines.

Data from de Castro and Kauffman (1998) was intentionally left out of calculations given the broad range of site descriptions. Also, two outliers (due to their heavier fuel loads) tended to dominate and influence the correlations. Their points are shown on the graphs for comparative purposes.

An alternative approach was conducted, calculating grass fuel consumption and surface (non-grass) fuel consumption separately and then combining these afterwards. In dambo landscapes, the average grass fuel load was 2.18 t ha^{-1} and surface fuel load 1.83 t ha^{-1}. In miombo, the average grass fuel load was 1.06 t ha^{-1} and the surface fuel load 8.13 t ha^{-1}. While this approach improved the correlations, the separation from the line of equality remained (not shown). To better match to the average fuel consumption values, the fuel loads were adjusted to correct for the bias, as shown in Figure A.10, bringing the predictions in line with the observed values. Correlation values (r^2) were 0.330 for dambo grassland and 0.709 for miombo woodland.

The GFED model describes dambo as grassland savanna and uses a 5.3 t ha^{-1} fuel load with an 81% combustion completeness resulting in 0.43 kg m^{-2} fuel consumption. It describes miombo as woody savanna with a 11 t ha^{-1} fuel load,

58% combustion completeness and 0.51 kg m^{-2} fuel consumption. These relations are shown as horizontal lines of constant

975   prediction for comparison purposes. Admittedly, the GFFEPS predictions are a modest improvement over the constant values

for the GFED predictions, but this is a result of the high variability of the fuel loads in the source material. It does indicate

GFED predictions are 10 to 20% or more higher than GFFEPS. Given the frequency of fire on the African savanna, such a

difference would amount to substantially higher emissions in GFED predictions. Finally, we note the need for further studies

of fire behaviour over a wider range of conditions in this region, in order to evaluate weather-based models such as ours.
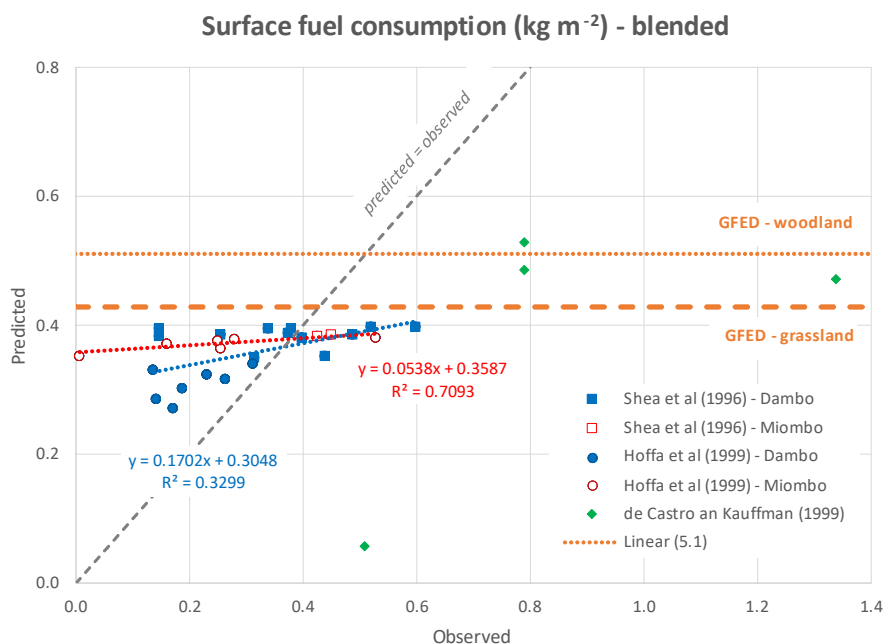
980

Figure A.10. Predicted vs observed fuel consumption in savanna landscape using the modified fuel consumption approach. Three separate studies are shown. The constant values of GFED predictions (0.43 and 0.51 kg/m^2) are shown as an orange dashed lines.

A.5 Australia Eucalypt Forests

985   Over 22% of Australia is forested, of which 78% is Eucalypt (Sullivan et al. 2012). Eucalypt (Jarrah) does not fit the

typical fire behaviour reflected in the Canadian system so an effort was made to create a fuel consumption model specific to

eucalypt from the published literature. In 1983, Australian agencies conducted the Aquarius project. This project studied a

number of aspects of fire in dry eucalypt forests, including fire behaviour, fire line productivity and workers' safety and health

(Budd et al. 1997).

990 Hollis et al. (2010) summarized woody fuel consumption in eucalypt fires for 18 of the 32 fires of project Aquarius (among other fires) at McCorkhill forest block (33°56′38″S, 115°31′52″E as reported in Burrows et al, 2019). Dates for these fires were collected from Cheney et al. (2012) and from Gould (pers. comm. 2022). *BUI*s were then ascertained from 1983 re-analysis data (McElhinny et al. 2020). Sigmoidal curves similar in structure to those used in the Canadian Forest Fire Behaviour Prediction (FBP) System were used. An upper limit of 90% was used as it was assumed that standing snags would

995 likely be left after a fire-front passage. This is supported by the highest reported observation in the Aquarius studies. As sigmoid curve fitting is inexact, four models were constructed based on successive power increments and a minimization of the sum of residuals. Figure A.11 shows the chosen, resulting curve. The choice of best model fit is speculative, given the spread of the data and the closeness of the curves.
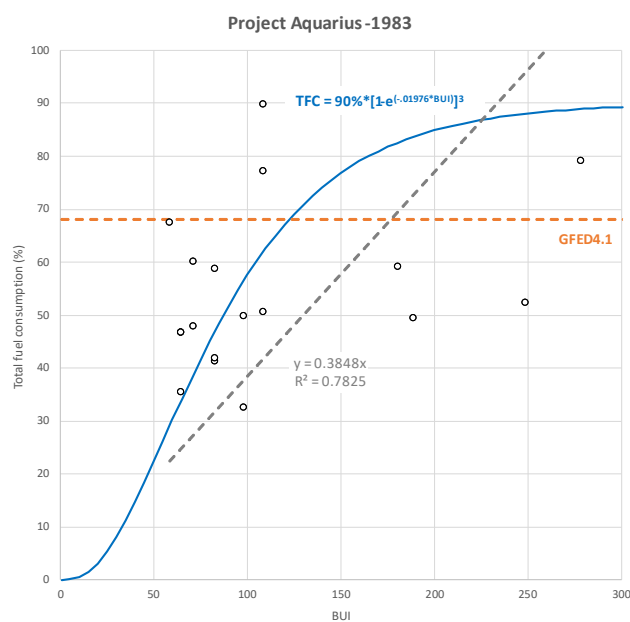
1000 **Figure A.11. Total fuel consumption in dry eucalypt forests based on Project Aquarius observations. Data points for 18 Aquarius fires are labelled. A linear regression through the origin shown as a dashed line. A sigmoidal curve shows the chosen fit based on successive power increments. The constant value of GFED predictions (68.1%) is shown as an orange dashed line.**

1005 For eucalyptus, GFED reports an average combustion completeness of 66% (shown on the figure) and fuel consumption of 7.9 kg m^{-2}.

It is worth noting that the fire sites reported in Project Aquarius reflect the coarse woody debris left from forest management practices. This is evident in some of the other sites reported by Hollis et al. (2010), with pre-fire woody fuel loads in excess of 1000 t ha^{-1} at Warra, Tasmania – a wet eucalypt forest site. Sullivan et al. (2012) reports a typical fuel load of 78 t ha^{-1} in Jarrah (tall understorey), matching the average of all dry eucalypt sites in Hollis et al. (2010). This value was then assumed for all Australian forests.

Another factor to address is forest coverage. Oliveira et al. (2015) examined fire activity in tropical savannas in northern Australia. They described the landscapes as open woodlands, woodlands, and open forests with forest protective covers of <10%, 10-30% and 30-70% respectively. Average values of these were used in GFFEPS, with balance as grass fuels following the blended approach used in savanna.

Code and data availability. The data used in the analysis presented herein, and the GFFEPS code, are available online at https://zenodo.org/doi/10.5281/zenodo.10710452.

Author contributions. K.A.: research and development of GFFEPS, testing of code, manuscript preparation. J.C.: preparation of meteorological data, compile and execute GFFEPS for the study period, manuscript review and editorial contributions. P.E.: preparation of hotspot fields, development and documentation of hotspot methodology. D.G.: manuscript review and editorial contributions. P.A.M.: project management, manuscript review and editorial contributions. D.T.: review and assistance in development of GFFEPS equations and methodology, manuscript review and editorial contributions.

Competing interests. The authors declare that they have no conflict of interest.

9 References

Abram, N.J., Henley, B.J., Sen Gupta, A., Lippmann, T.J., Clarke, H., Dowdy, A.J., Sharples, J.J., Nolan, R.H., Zhang, T., Wooster, M.J. and Wurtzel, J.B.: Connections of climate change and variability to large and extreme forest fires in southeast Australia. Communications Earth & Environment, 2(1), p.8, 2021.

Adams, C., McLinden, C.A., Shephard, M.W., Dickson, N., Dammers, E., Chen, J., Makar, P., Cady-Pereira, K.E., Tam, N., Kharol, S.K. and Lamsal, L.N.: Satellite-derived emissions of carbon monoxide, ammonia, and nitrogen dioxide from the 2016 Horse River wildfire in the Fort McMurray area. Atmospheric Chemistry and Physics, 19(4), pp.2577-2599, 2019.

Akagi, S.K., Yokelson, R.J., Wiedinmyer, C., Alvarado, M.J., Reid, J.S., Karl, T., Crounse, J.D. and Wennberg, P.O.: Emission factors for open and domestic biomass burning for use in atmospheric models. Atmospheric Chemistry and Physics, 11(9), pp.4039-4072, 2011.

Alexander, M.E.: Foliar moisture content input in the Canadian Forest Fire Behavior Prediction System for areas outside of
1040   Canada. In VI International Conference on Forest Fire Research (pp. 15-18), 2010a.

Alexander, M.E.: Surface fire spread potential in trembling aspen during summer in the Boreal Forest Region of Canada. The
Forestry Chronicle, 86(2), pp.200-212, 2010b.

Alexander, M.E., Stocks, B.J. and Lawson, B.D.:. Fire behavior in black spruce-lichen woodland: the Porter Lake project (No.
NOR-X-310). Forestry Canada-Northwest Region, 1990

1045   Anderson, K.R., Englefield, P., Little, J.M. and Reuter, G.: An approach to operational forest fire growth predictions for
Canada. International Journal of Wildland Fire, 18(8), pp.893-905, 2009.

Anderson, K.R.: January. Incorporating smoldering into fire growth modelling. In Third Symposium on Fire and Forest
Meteorology (pp. 9-14), 2000,

Ban, Y., Zhang, P., Nascetti, A., Bevington, A.R. and Wulder, M.A.: Near real-time wildfire progression monitoring with
1050   Sentinel-1 SAR time series and deep learning. Scientific reports, 10(1), p.1322, 2020.

Barros, B., Oliveira, M. and Morais, S.: Continent-based systematic review of the short-term health impacts of wildfire
emissions. Journal of Toxicology and Environmental Health, Part B, 26(7), pp.387-415, 2023.

Bartholome, E. and Belward, A.S.: GLC2000: a new approach to global land cover mapping from Earth observation data.
International Journal of Remote Sensing, 26(9), pp.1959-1977, 2005.

1055   Budd, G.M., Brotherhood, J.R., Hendrie, A.L., Jeffery, S.E., Beasley, F.A., Costin, B.P., Zhien, W., Baker, M.M., Cheney,
N.P. and Dawson, M.P.: Project Aquarius 1. Stress, strain, and productivity in men suppressing Australian summer
bushfires with hand tools: background, objectives, and methods. International Journal of Wildland Fire, 7(2), pp.69-76,
1997.

Burrows, N., Ward, B., Wills, A., Williams, M. and Cranfield, R.: Fine-scale temporal turnover of jarrah forest understory
1060   vegetation assemblages is independent of fire regime. Fire Ecology, 15(1), pp.1-18, 2019.

Bond, T.C., Doherty, S.J., Fahey, D.W., Forster, P.M., Berntsen, T., DeAngelo, B.J., Flanner, M.G., Ghan, S., Kärcher, B.,
Koch, D. and Kinne, S.: Bounding the role of black carbon in the climate system: A scientific assessment. Journal of
geophysical research: Atmospheres, 118(11), pp.5380-5552, 2013.

Carvalho Jr, J.A., Santos, J.M., Santos, J.C.D., Leitão, M.M. and Higuchi, N.: A tropical rainforest clearing experiment by
1065   biomass burning in the Manaus region. Atmospheric Environment, 29(17), pp.2301-2309, 1995.

Cassou, E.: Field Burning (English). Agricultural Pollution. Washington, DC: World Bank Group, 2018.

Chen, G., Guo, Y., Yue, X., Tong, S., Gasparrini, A., Bell, M.L., Armstrong, B., Schwartz, J., Jaakkola, J.J., Zanobetti, A. and
Lavigne, E.: Mortality risk attributable to wildfire-related PM2· 5 pollution: a global time series study in 749 locations.
The Lancet Planetary Health, 5(9), pp.e579-e587, 2021.

1070   Chen, J., Anderson, K., Pavlovic, R., Moran, M.D., Englefield, P., Thompson, D.K., Munoz-Alpizar, R. and Landry, H.: The
FireWork v2. 0 air quality forecast system with biomass burning emissions from the Canadian Forest Fire Emissions
Prediction System v2. 03. Geoscientific Model Development, 12(7), pp.3283-3310, 2019.

Chen, Y., Hall, J., van Wees, D., Andela, N., Hantson, S., Giglio, L., van der Werf, G.R., Morton, D.C. and Randerson, J.T.: Multi-decadal trends and variability in burned area from the 5th version of the Global Fire Emissions Database (GFED5). Earth System Science Data Discussions, 2023, pp.1-52, 2023.

Countryman, C.M.: The fire environment concept. Pacific Southwest Forest and Range Experiment Station, 1972.

Cheney, N.P., Gould, J.S., McCaw, W.L. and Anderson, W.R.: Predicting fire behaviour in dry eucalypt forest in southern Australia. Forest Ecology and Management, 280, pp.120-131, 2012.

De Castro, E.A. and Kauffman, J.B.: Ecosystem structure in the Brazilian Cerrado: a vegetation gradient of aboveground biomass, root mass and consumption by fire. Journal of tropical ecology, 14(3), pp.263-283, 1998.

Eyth, A., Vukovich, J., Farkas, C. and Godfrey, J.: Technical Support Document (TSD): Preparation of Emissions Inventories for the 2016v3 North American Emissions Modeling Platform. US Environmental Protection Agency, Office of Air Quality Planning and Standards, Air Quality Assessment Division, 2022.

Field, R.D., Van Der Werf, G.R. and Shen, S.S.: Human amplification of drought-induced biomass burning in Indonesia since 1960. Nature Geoscience, 2(3), pp.185-188, 2009.

Fearnside, P.M., Leal Jr, N. and Fernandes, F.M.: Rainforest burning and the global carbon budget: biomass, combustion efficiency, and charcoal formation in the Brazilian Amazon. Journal of Geophysical Research: Atmospheres, 98(D9), pp.16733-16743, 1993.

Fearnside, P.M., de Alencastro Graça, P.M.L. and Rodrigues, F.J.A.: Burning of Amazonian rainforests: burning efficiency and charcoal formation in forest cleared for cattle pasture near Manaus, Brazil. Forest Ecology and Management, 146(1-3), pp.115-128, 2001.

Field, R.D., Wang, Y. and Roswintiarti, O.: A drought-based predictor of recent haze events in western Indonesia. Atmospheric Environment, 38(13), pp.1869-1878, 2004.

Forestry Canada Fire Danger Group: Development and structure of the Canadian forest fire behavior prediction system (Vol. 3). Forestry Canada, Science and Sustainable Development Directorate, 1992.

Friedlingstein, P., O'sullivan, M., Jones, M.W., Andrew, R.M., Gregor, L., Hauck, J., Le Quéré, C., Luijkx, I.T., Olsen, A., Peters, G.P. and Peters, W.: Global carbon budget 2022. Earth System Science Data Discussions, 2022, pp.1-159, 2022.

Gaveau, D.L., Descals, A., Salim, M.A., Sheil, D. and Sloan, S.: Refined burned-area mapping protocol using Sentinel-2 data increases estimate of 2019 Indonesian burning. Earth System Science Data, 13(11), pp.5353-5368, 2021.

Giglio, L., Van der Werf, G.R., Randerson, J.T., Collatz, G.J. and Kasibhatla, P.: Global estimation of burned area using MODIS active fire observations. Atmospheric Chemistry and Physics, 6(4), pp.957-974, 2006.

Giglio, L., Schroeder, W. and Justice, C.O.: The collection 6 MODIS active fire detection algorithm and fire products. Remote sensing of environment, 178, pp.31-41, 2016.

Goodenough, D.G., Chen, H., Richardson, A., Cloude, S., Hong, W. and Li, Y.: Mapping fire scars using Radarsat-2 polarimetric SAR data. Canadian Journal of Remote Sensing, 37(5), pp.500-509, 2011.

Graham, L.L., Applegate, G.B., Thomas, A., Ryan, K.C., Saharjo, B.H. and Cochrane, M.A.: A Field Study of Tropical Peat Fire Behaviour and Associated Carbon Emissions. Fire, 5(3), p.62, 2022.

Griffin, D., Sioris, C., Chen, J., Dickson, N., Kovachik, A., Graaf, M.D., Nanda, S., Veefkind, P., Dammers, E., McLinden, C.A. and Makar, P.: The 2018 fire season in North America as seen by TROPOMI: aerosol layer height intercomparisons and evaluation of model-derived plume heights. Atmospheric Measurement Techniques, 13(3), pp.1427-1445, 2020.

Griffin, D., Chen, J., Anderson, K., Makar, P., McLinden, C.A., Dammers, E. and Fogal, A.: Towards an improved understanding of wildfire CO emissions: a satellite remote-sensing perspective. EGUsphere, 2023, pp.1-37.Huang, M., Carmichael, G.R., Pierce, R.B., Jo, D.S., Park, R.J., Flemming, J., Emmons, L.K., Bowman, K.W., Henze, D.K., Davila, Y. and Sudo, K., 2017. Impact of intercontinental pollution transport on North American ozone air pollution: an HTAP phase 2 multi-model study. Atmospheric chemistry and physics, 17(9), pp.5721-5750, 2023.

Guild, L.S., Kauffman, J.B., Ellingson, L.J., Cummings, D.L., Castro, E.A., Babbitt, R.E. and Ward, D.E.: Dynamics associated with total aboveground biomass, C, nutrient pools, and biomass burning of primary forest and pasture in Rondonia, Brazil during SCAR-B. Journal of Geophysical Research: Atmospheres, 103(D24), pp.32091-32100, 1998.

Hatch, L.E., Yokelson, R.J., Stockwell, C.E., Veres, P.R., Simpson, I.J., Blake, D.R., Orlando, J.J. and Barsanti, K.C.: Multi-instrument comparison and compilation of non-methane organic gas emissions from biomass burning and implications for smoke-derived secondary organic aerosol precursors. Atmospheric Chemistry and Physics, 17(2), pp.1471-1489, 2017.

Hayden, K.L., Li, S.M., Liggio, J., Wheeler, M.J., Wentzell, J.J., Leithead, A., Brickell, P., Mittermeier, R.L., Oldham, Z., Mihele, C.M. and Staebler, R.M.: Reconciling the total carbon budget for boreal forest wildfire emissions using airborne observations. Atmospheric Chemistry and Physics, 22(18), pp.12493-12523, 2022.

Hoffa, E.A., Ward, D.E., Hao, W.M., Susott, R.A. and Wakimoto, R.H.: Seasonality of carbon emissions from biomass burning in a Zambian savanna. Journal of Geophysical Research: Atmospheres, 104(D11), pp.13841-13853, 1999.

Hollis, J.J., Matthews, S., Ottmar, R.D., Prichard, S.J., Slijepcevic, A., Burrows, N.D., Ward, B., Tolhurst, K.G., Anderson, W.R. and Gould, J.S.: Testing woody fuel consumption models for application in Australian southern eucalypt forest fires. Forest Ecology and Management, 260(6), pp.948-964, 2010.

Huijnen, V., Wooster, M.J., Kaiser, J.W., Gaveau, D.L., Flemming, J., Parrington, M., Inness, A., Murdiyarso, D., Main, B. and van Weele, M.: Fire carbon emissions over maritime southeast Asia in 2015 largest since 1997. Scientific reports, 6(1), p.26886, 2016.

Jolly, W.M., Nemani, R. and Running, S.W.: A generalized, bioclimatic index to predict foliar phenology in response to climate. Global Change Biology, 11(4), pp.619-632, 2005.

Kaiser, J.W., Heil, A., Andreae, M.O., Benedetti, A., Chubarova, N., Jones, L., Morcrette, J.J., Razinger, M., Schultz, M.G., Suttie, M. and Van Der Werf, G.R.: Biomass burning emissions estimated with a global fire assimilation system based on observed fire radiative power. Biogeosciences, 9(1), pp.527-554, 2012.

1140 Kaiser, J. W. and van der Werf, G. R.: Biomass burning [in "State of the Climate in 2018"]. Bull. Amer. Meteor. Soc., 100
       (9), S64–S65, doi:10.1175/2019BAMSStateoftheClimate.1, 2019.

Kaiser, J. W. and van der Werf, G. R.: Biomass burning [in "State of the Climate in 2021"]. Bull. Amer. Meteor. Soc., 103
       (8), S103–S105, https://doi.org/10.1175/BAMS-D-22-0092.1, 2022.

Kaiser, J.W., van der Werf, G.R., and Heil, A.: Biomass burning. Bulletin of the American Meteorological Society, Spec.
1145   Suppl." State of the Climate in 2015", 97(8), pp.S60-S62, 2016.

Kauffman, J.B., Sanford Jr, R.L., Cummings, D.L., Salcedo, I.H. and Sampaio, E.V.S.B.: Biomass and nutrient dynamics
       associated with slash fires in neotropical dry forests. Ecology, 74(1), pp.140-151, 1993.

Kauffman, J.B., Cummings, D. L., & Ward, D. E.: Fire in the Brazilian Amazon 2. Biomass, nutrient pools and losses in cattle
       pastures. Oecologia, 113, 415-427, 1998.

1150 Keeley, J.E. and Syphard, A.D.: Large California wildfires: 2020 fires in historical context. Fire Ecology, 17(1), pp.1-11.

Knorr, W., Lehsten, V. and Arneth, A., 2012. Determinants and predictability of global wildfire emissions. Atmospheric
       Chemistry and Physics, 12(15), pp.6845-6861, 2021.

Lee, B.S., Alexander, M.E., Hawkes, B.C., Lynham, T.J., Stocks, B.J. and Englefield, P.: Information systems in support of
       wildland fire management decision making in Canada. Computers and Electronics in Agriculture, 37(1-3), pp.185-198,
1155   2002.

Liu, Y., Huang, Y., Liggio, J., Hayden, K., Mihele, C., Wentzell, J., Wheeler, M., Leithead, A., Moussa, S., Xie, C. and Yang,
       Y.: A newly developed Lagrangian chemical transport scheme: Part 1. Simulation of a boreal forest fire plume. Science
       of The Total Environment, 880, p.163232, 2023.

Lowrie, M., "Forest fire centre declares 2023 worst year ever for Canadian wildfires." The Globe and Mail, June 26, 2023,
1160   https://www.theglobeandmail.com/canada/article-quebec-wildfire-smoke-causes-widespread-smog-warnings-
       grounds-some/, 2023

Makar, P.A., Akingunola, A., Chen, J., Pabla, B., Gong, W., Stroud, C., Sioris, C., Anderson, K., Cheung, P., Zhang, J. and
       Milbrandt, J.: Forest Fire Aerosol–Weather Feedbacks over Western North America Using a High-Resolution, Fully
       Coupled, Air quality Model. Atmospheric Chemistry and Physics Discussions, pp.1-55, 2020.

1165 Matz, C.J., Egyed, M., Xi, G., Racine, J., Pavlovic, R., Rittmaster, R., Henderson, S.B. and Stieb, D.M.: Health impact analysis
       of PM2. 5 from wildfire smoke in Canada (2013–2015, 2017–2018). Science of The Total Environment, 725, p.138506,
       2020.

McCarty, J.L., Korontzi, S., Justice, C.O. and Loboda, T.: The spatial and temporal distribution of crop residue burning in the
       contiguous United States. Science of the Total Environment, 407(21), pp.5701-5712, 2009.

1170 McElhinny, M., Beckers, J.F., Hanes, C., Flannigan, M. and Jain, P.: A high-resolution reanalysis of global fire weather from
       1979 to 2018–overwintering the Drought Code. Earth System Science Data, 12(3), pp.1823-1833, 2020.

McRae, D.J., Conard, S.G., Ivanova, G.A., Sukhinin, A.I., Baker, S.P., Samsonov, Y.N., Blake, T.W., Ivanov, V.A., Ivanov, A.V., Churkina, T.V. and Hao, W.: Variability of fire behavior, fire effects, and emissions in Scotch pine forests of Central Siberia. Mitigation and Adaptation Strategies for Global Change, 11(1), pp.45-74, 2006.

1175 Mota, B. and Wooster, M.J.: A new top-down approach for directly estimating biomass burning emissions and fuel consumption rates and totals from geostationary satellite fire radiative power (FRP). Remote sensing of environment, 206, pp.45-62, 2018.

Oliveira, S.L., Maier, S.W., Pereira, J.M. and Russell-Smith, J.: Seasonal differences in fire activity and intensity in tropical savannas of northern Australia using satellite measurements of fire radiative power. International Journal of Wildland

1180 Fire, 24(2), pp.249-260, 2015.

Quintilio, D., Alexander, M.E. and Ponto, R.L.: Spring fires in a semimature trembling aspen stand in central Alberta (No. NOR-X-323). Forestry Canada-Northwest Region, 1991.

Nguyen, H.M. and Wooster, M.J.: Advances in the estimation of high Spatio-temporal resolution pan-African top-down biomass burning emissions made using geostationary fire radiative power (FRP) and MAIAC aerosol optical depth

1185 (AOD) data. Remote Sensing of Environment, 248, p.111971, 2020.

Page, S.E. and Hooijer, A.: In the line of fire: the peatlands of Southeast Asia. Philosophical Transactions of the Royal Society B: Biological Sciences, 371(1696), p.20150176, 2016.

Pan, X., Ichoku, C., Chin, M., Bian, H., Darmenov, A., Colarco, P., Ellison, L., Kucsera, T., Silva, A.D., Wang, J. and Oda, T.: Six global biomass burning emission datasets: intercomparison and application in one global aerosol model.

1190 Atmospheric Chemistry and Physics, 20(2), pp.969-994, 2020.

Pettorelli, N.: The normalized difference vegetation index. Oxford University Press, USA, 2013.

Pereira, G., Longo, K.M., Freitas, S.R., Mataveli, G., Oliveira, V.J., Santos, P.R., Rodrigues, L.F. and Cardozo, F.S.: Improving the south America wildfires smoke estimates: Integration of polar-orbiting and geostationary satellite fire products in the Brazilian biomass burning emission model (3BEM). Atmospheric Environment, 273, p.118954, 2022.

1195 Pearce, H.G., Anderson, S.A.J. and Clifford, V.R.: A manual for predicting fire behaviour in New Zealand fuels. Scion Rural Fire Research Group, 2008.

Pouliot, G., Rao, V., McCarty, J.L. and Soja, A.: Development of the crop residue and rangeland burning in the 2014 National Emissions Inventory using information from multiple sources. Journal of the Air & Waste Management Association, 67(5), pp.613-622, 2017.

1200 Ramo, R., Roteta, E., Bistinas, I., Van Wees, D., Bastarrika, A., Chuvieco, E. and Van der Werf, G.R.: African burned area and fire carbon emissions are strongly impacted by small fires undetected by coarse resolution satellite data. Proceedings of the National Academy of Sciences, 118(9), p.e2011160118, 2021.

Randerson, J.T., Chen, Y., Van Der Werf, G.R., Rogers, B.M. and Morton, D.C.: Global burned area and biomass burning emissions from small fires. Journal of Geophysical Research: Biogeosciences, 117(G4) , 2012.

1205 Roberts, G. and Wooster, M.J.: Global impact of landscape fire emissions on surface level PM2. 5 concentrations, air quality exposure and population mortality. Atmospheric Environment, 252, p.118210, 2021.

Schmidt, I.B. and Eloy, L.: Fire regime in the Brazilian Savanna: Recent changes, policy and management. Flora, 268, p.151613, 2020.

Seiler, W. and Crutzen, P.J.: Estimates of gross and net fluxes of carbon between the biosphere and the atmosphere from
1210 biomass burning. Climatic change, 2(3), pp.207-247, 1980.

Shea, R.W., Shea, B.W., Kauffman, J.B., Ward, D.E., Haskins, C.I. and Scholes, M.C.: Fuel biomass and combustion factors associated with fires in savanna ecosystems of South Africa and Zambia. Journal of Geophysical Research: Atmospheres, 101(D19), pp.23551-23568, 1996.

Stocks, B.J.: Fire behavior in immature jack pine. Canadian Journal of Forest Research, 17(1), pp.80-86, 1987.

1215 Stocks, B.J.: Fire potential in the spruce budworm-damaged forests of Ontario. The Forestry Chronicle, 63(1), pp.8-14, 1987.

Stocks, B.J.: Fire behavior in mature jack pine. Canadian Journal of Forest Research, 19(6), pp.783-790, 1989.

Stocks, B.J., Alexander, M.E., Wotton, B.M., Stefner, C.N., Flannigan, M.D., Taylor, S.W., Lavoie, N., Mason, J.A., Hartley, G.R., Maffey, M.E. and Dalrymple, G.N.: Crown fire behaviour in a northern jack pine black spruce forest. Canadian Journal of Forest Research, 34(8), pp.1548-1560, 2004.

1220 Stocks, B.J., Lynham, T.J., Lawson, B.D., Alexander, M.E., Wagner, C.V., McAlpine, R.S. and Dube, D.E. Canadian forest fire danger rating system: an overview. The Forestry Chronicle, 65(4), pp.258-265, 1989.

Stockwell, C.E., Bela, M.M., Coggon, M.M., Gkatzelis, G.I., Wiggins, E., Gargulinski, E.M., Shingler, T., Fenn, M., Griffin, D., Holmes, C.D. and Ye, X.: Airborne emission rate measurements validate remote sensing observations and emission inventories of western US wildfires. Environmental science & technology, 56(12), pp.7564-7577, 2022.

1225 Streets, D.G., Yarber, K.F., Woo, J.H. and Carmichael, G.R.: Biomass burning in Asia: Annual and seasonal estimates and atmospheric emissions. Global Biogeochemical Cycles, 17(4) , 2003.

Sullivan, A.L., McCaw, W.L., Cruz, M.G., Matthews, S. and Ellis, P.F.: Fuel, fire weather and fire behaviour in Australian ecosystems. Flammable Australia: fire regimes, biodiversity and ecosystems in a changing world, pp.51-77, 2012.

Swart, N.C., Cole, J.N., Kharin, V.V., Lazare, M., Scinocca, J.F., Gillett, N.P., Anstey, J., Arora, V., Christian, J.R., Hanna,
1230 S. and Jiao, Y.: The Canadian earth system model version 5 (CanESM5. 0.3). Geoscientific Model Development, 12(11), pp.4823-4873, 2019.

Taylor, S.W. and Alexander, M.E.: Science, technology, and human factors in fire danger rating: the Canadian experience. International Journal of Wildland Fire, 15(1), pp.121-135, 2006.

Thomas, S.C. and Martin, A.R.: Carbon content of tree tissues: a synthesis. Forests, 3(2), pp.332-352, 2012.

1235 Thompson, D.K., Simpson, B.N., Whitman, E., Barber, Q.E. and Parisien, M.A.: Peatland hydrological dynamics as a driver of landscape connectivity and fire activity in the boreal plain of Canada. Forests, 10(7), p.534, 2019.

Tubiello, F.N., Salvatore, M., Cóndor Golec, R.D., Ferrara, A., Rossi, S., Biancalani, R., Federici, S., Jacobs, H. and Flammini, A.: Agriculture, forestry and other land use emissions by sources and removals by sinks. Rome, Italy, 2014.

Turn, S.Q., Jenkins, B.M., Chow, J.C., Pritchett, L.C., Campbell, D., Cahill, T. and Whalen, S.A.: Elemental characterization
1240   of particulate matter emitted from biomass burning: Wind tunnel derived source profiles for herbaceous and wood fuels.
         Journal of Geophysical Research: Atmospheres, 102(D3), pp.3683-3699, 1997.

Urbanski, S.: Wildland fire emissions, carbon, and climate: Emission factors. Forest Ecology and Management, 317, pp.51-
         60, 2014.

van der Werf, G.R., Randerson, J.T., Giglio, L., Leeuwen, T.T.V., Chen, Y., Rogers, B.M., Mu, M., Van Marle, M.J., Morton,
1245   D.C., Collatz, G.J. and Yokelson, R.J.: Global fire emissions estimates during 1997–2016. Earth System Science Data,
         9(2), pp.697-720, 2017.

van Leeuwen, T.T., van der Werf, G.R., Hoffmann, A.A., Detmers, R.G., Rücker, G., French, N.H., Archibald, S., Carvalho
         Jr, J.A., Cook, G.D., de Groot, W.J. and Hély, C.: Biomass burning fuel consumption rates: a field measurement
         database. Biogeosciences, 11(24), pp.7305-7329, 2014.

1250 van Wagner, C.E. and Forest, P.: Development and structure of the Canadian Forest Fire Weather Index System. In Can. For.
         Serv., Forestry Tech. Rep., 1987.

van Wees, D., van der Werf, G.R., Randerson, J.T., Rogers, B.M., Chen, Y., Veraverbeke, S., Giglio, L. and Morton, D.C.
         Global biomass burning fuel consumption and emissions at 500 m spatial resolution based on the Global Fire Emissions
         Database (GFED). Geoscientific Model Development, 15(22), pp.8411-8437, 2022.

1255 Vaughan, G., Draude, A.P., Ricketts, H., Schultz, D.M., Adam, M., Sugier, J. and Wareing, D.P.: Transport of Canadian forest
         fire smoke over the UK as observed by lidar. Atmospheric Chemistry & Physics, 18(15) , 2018.

Vitolo, C., Di Giuseppe, F., Barnard, C., Coughlan, R., San-Miguel-Ayanz, J., Libertá, G. and Krzeminski, B.: ERA5-based
         global meteorological wildfire danger maps. Scientific data, 7(1), p.216, 2020.

von Salzen, K., Scinocca, J.F., McFarlane, N.A., Li, J., Cole, J.N., Plummer, D., Verseghy, D., Reader, M.C., Ma, X., Lazare,
1260   M. and Solheim, L.: The Canadian fourth generation atmospheric global climate model (CanAM4). Part I:
         representation of physical processes. In Data, Models and Analysis (pp. 123-144). Routledge, 2019.

Ward, D.E., Susott, R., Kauffman, J.B., Babbitt, R.E., Cummings, D.L., Dias, B., Holben, B.N., Kaufman, Y.J., Rasmussen,
         R.A. and Setzer, A.W.: Smoke and fire characteristics for cerrado and deforestation burns in Brazil: BASE-B
         experiment. Journal of Geophysical Research: Atmospheres, 97(D13), pp.14601-14619, 1992.

1265 Wentworth, G.R., Aklilu, Y.A., Landis, M.S. and Hsu, Y.M.: Impacts of a large boreal wildfire on ground level atmospheric
         concentrations of PAHs, VOCs and ozone. Atmospheric Environment, 178, pp.19-30, 2018.

Wiedinmyer, C., Akagi, S.K., Yokelson, R.J., Emmons, L.K., Al-Saadi, J.A., Orlando, J.J. and Soja, A.J.: The Fire INventory
         from NCAR (FINN): A high resolution global model to estimate the emissions from open burning. Geoscientific Model
         Development, 4(3), pp.625-641, 2011.

1270 Wiedinmyer, C., Kimura, Y., McDonald-Buller, E.C., Emmons, L.K., Buchholz, R.R., Tang, W., Seto, K., Joseph, M.B.,
         Barsanti, K.C., Carlton, A.G. and Yokelson, R.: The Fire Inventory from NCAR version 2.5: An updated global fire
         emissions model for climate and chemistry applications. EGUsphere, 2023, pp.1-45, 2023.

Withey, K., Berenguer, E., Palmeira, A.F., Espírito-Santo, F.D., Lennox, G.D., Silva, C.V., Aragão, L.E., Ferreira, J., França, F., Malhi, Y. and Rossi, L.C.: Quantifying immediate carbon emissions from El Niño-mediated wildfires in humid tropical forests. Philosophical Transactions of the Royal Society B: Biological Sciences, 373(1760), p.20170312 , 2018.

Wotton, B.M., Alexander, M.E. and Taylor, S.W.: Updates and revisions to the 1992 Canadian forest fire behavior prediction system. Great Lakes Forestry Centre, 2009.

Wu, Y., Peña, W., Gross, B. and Moshary, F.: Wildfire smoke transport and impact on air quality observed by a mullti-wavelength elastic-raman lidar and ceilometer in New York city. In EPJ Web of Conferences (Vol. 176, p. 05044). EDP Sciences, 2018.

Zhang, T., Wooster, M.J., De Jong, M.C. and Xu, W.: How well does the 'small fire boost'methodology used within the GFED4. 1s fire emissions database represent the timing, location and magnitude of agricultural burning? Remote Sensing, 10(6), p.823, 2018.